1-1-2015

Physical Layer Algorithms for Interference Reduction in OFDM-Based Cognitive Radio Systems

Anas Tom
University of South Florida, atom@mail.usf.edu

Physical Layer Algorithms for Interference Reduction in OFDM-Based Cognitive Radio Systems

by

Anas Tom

A dissertation submitted in partial fulfillment
of the requirements for the degree of
Doctor of Philosophy
Department of Electrical Engineering
College of Engineering
University of South Florida

Major Professor: Hüseyin Arslan, Ph.D.
Richard D. Gitlin, Sc.D.
Thomas Weller, Ph.D.
Alex Savachkin, Ph.D.
Rui Yang, Ph.D.

Date of Approval:
Februrary 18, 2015

Keywords: Alignment, out-of-band power leakage, peak-to-average power ratio, sidelobe suppression, spectrum shaping

DEDICATION

To my family

ACKNOWLEDGMENTS

I would like to thank my advisor Dr. Hüseyin Arslan for his support and guidance. I'm deeply indebted to him for giving me the opportunity to work with him and be part of his group. I would also like to express my deepest gratitude to Dr. Richard D. Gitlin, Dr. Thomas Weller, Dr. Alex Savachkin and Dr. Rui Yang for agreeing to be part of the committee and Dr. Dmitry Goldgof for chairing my dissertation defense.

During my PhD, I have had the privilege to work with many graduate students in the Wireless Communications and Signal Processing (WCSP) Group, I would like to thank all of them for being great colleagues and friends. I owe Special thanks to Dr. Alphan Sahin for the long and fruitful discussions while he was at USF or over Skype when he moved to Texas A&M.

I'm very grateful for the Electrical Engineering department staff, Gayla Montgomery, Irene Wiley, Jessica Procko, Cherie Dilley and Judy Hyde, for their patience and support with various administrative issues. I would also like to acknowledge the financial support provided by the Electrical Engineering department through teaching assistantships throughout my entire PhD, and in particular I would like to thank Dr. Paris Wiley for his support.

TABLE OF CONTENTS

LIST OF TABLES

LIST OF FIGURES

ABSTRACT

Orthogonal Frequency Division Multiplexing (OFDM) is a multi-carrier transmission scheme used in most of the existing wireless standards such as LTE, WiFi and WiMAX. The popularity of OFDM stems from the multitude of benefits it offers in terms of providing high data rate transmission, robustness against multipath fading and ease of implementation. Additionally, OFDM signals are agile in the sense that any subcarrier can be switched on or off to fit the available transmission bandwidth, which makes it well suited for systems with dynamic spectrum access such as cognitive radio systems. Nonetheless, and despite all the aforementioned advantages, OFDM signals have high spectral sidelobes outside the designated band of transmission, that can create severe interference to users in adjacent transmission bands, particularly when there is no synchronization between users. The focus of this dissertation is to propose baseband solutions at the Physical Layer (PHY) of the communications system to address the interference resulting from the high out-of-band (OOB) emissions of OFDM.

In the first part of this dissertation, we propose a precoder capable of generating mask compliant OFDM signals with low OOB emissions that are always contained under a given spectrum emission mask (SEM) specified by the OFDM standard. The proposed precoder generates transmitted signals with bit error rate (BER) performance similar to that of classical OFDM and does not reduce the spectral efficiency of the system.

In the second part of this dissertation, we introduce a novel and elegant approach, called *suppressing alignment* (SA), to jointly reduce the OOB interference and peak-to-average power ratio (PAPR) of OFDM systems. SA exploits the unavoidable redundancy provided by the CP as well as the wireless communications channel to generate an OOB/PAPR suppressing signal at the OFDM transmitter. Furthermore, after passing through the wireless channel, the suppressing signal is aligned with the CP duration at the OFDM receiver, essentially causing no interference to the

data portion of the OFDM symbol. The proposed approach improves the PAPR of the transmitted OFDM signal and reduces the OOB interference by tens of decibels. Additionally, the proposed approach maintains an error performance similar to that of plain OFDM without requiring any change in the receiver structure of legacy OFDM.

In order to reduce the spectral emissions of OFDM, additional blocks, such as linear precoders, are usually introduced in the transmitter leading to a transmitted signal that is drastically different than that of a classical OFDM signal. This distortion is typically quantified by the error vector magnitude (EVM), a widely used metric specified by the wireless standard and is directly related to the BER performance of the system. The receiver can usually decode the information data with acceptable error probabilities if the distortion introduced to the transmitted signal is below the EVM values specified in the OFDM standard. Linear precoders, while capable of achieving significant reduction in the OOB interference, they typically introduce large distortion to the transmitted signal. As such, the receiver needs to know the precoding done at the transmitter to be able to recover the data which usually entails sending large amount of side information that can greatly reduce the spectral efficiency of the system. In the last part of this dissertation, we target the design of precoders for the purpose reducing the OOB interference, in a transparent manner where the receiver does not need to know the changes introduced in the transmitter. We present two precoders capable of significantly reducing the OOB emissions while producing transmitted signals with EVM values below those specified by the wireless standard, thereby guaranteeing acceptable error performance.

CHAPTER 1

INTRODUCTION

1.1 Background and Motivation

The demand for high data rates has increased tremendously over the last decade due in part to the proliferation of multimedia services as well as the increased usage and availability of smart devices that enable such types of applications. This huge shift from voice-centric applications mandates a change in the way communications systems are designed. In particular, new technologies are needed that enable efficient utilization of the spectrum. The current static allocation of the spectrum is not well suited for such high increases in the data rates. The problem of not meeting the high demand in wireless broadband services has usually been attributed to the lack of spectrum resources. Nonetheless, several measurement campaigns conducted by the Federal Communication Commission (FCC) show significant underutilization of licensed frequency bands [3]. Therefore, what was originally viewed as a spectrum scarcity problem, is in reality an underutilization of spectrum resources. Such inefficient use of the radio spectrum can be completely avoided if opportunistic use of the licensed spectrum is allowed. The idea here is that, although the licensed spectrum is owned by some entity that has exclusive rights over the assigned frequency band, it should be allowed to be used by others whenever the legacy owner is idle. Such opportunistic access of the spectrum by unlicensed users can potentially create enough spectrum resources to meet the high data rates demand of next generation networks.

Motivated by these findings, *cognitive radio*, proposed by Mitola [4], has emerged as the enabling technology aimed at alleviating the problems arising from the static usage of the spectrum. A cognitive radio as envisioned by Mitola, is an intelligent radio that is aware of its surroundings, capable of sensing the environment, and able to adapt its transmission parameters accordingly.

Through the use of cognitive radio, a secondary user (SU) can detect unoccupied licensed frequency bands owned by a legacy user, also known as a primary user (PU), and utilize these frequencies temporarily [5]. However, such opportunistic access of the spectrum poses several technological challenges, particularity at the physical layer (PHY) of the wireless communications system. One major challenge is the ability of the radio of the SU to sense and detect idle frequency bands (also known as white spaces) not currently used by the PU. This is widely known as the spectrum sensing problem, which is very crucial to the operation of any cognitive radio system. A plethora of research has been dedicated to the spectrum sensing problem, readers can refer to [6] and the references therein for more information. The other major challenge, which is the focus of this dissertation, is related to the coexistence of opportunistic users and the legacy owners of the spectrum. Opportunistic access of the spectrum in a cognitive radio environment is based on the premise that the secondary opportunistic user causes minimal interference to the legacy primary users operating in adjacent bands. In fact, secondary access of the spectrum is allowed only under very strict interference requirements specified by regulatory agencies such as the FCC in the United States. Such interference requirements are usually specified in the form of a spectral emission mask (SEM). In this context, the transmitter of the secondary cognitive radio system should have low out-of-band (OOB) emissions that meet the spectral demands of the specified regulatory mask.

In addition to the OOB emissions requirement discussed above, the PHY layer of the cognitive radio should adopt an agile waveform, that can adaptively shape its spectrum. This is due to the fact that the white spaces are usually non-contiguous and scattered across the whole frequency band. An agile waveform would be able to fill and aggregate all white spaces (spectrum holes) not used by the primary system. Multicarrier schemes readily fullfil this requirement as they have the ability to null or turn-off subcarriers in locations where legacy users are transmitting. For this reason, several multicarrier waveforms, such as filter bank multicarrier (FBMC) [7], generalized frequency division multiplexing (GFDM) [8] and orthogonal frequency division multiplexing (OFDM) [9], were proposed for the PHY layer of cognitive radios. Although both FBMC and GFDM have very low OOB emissions compared to OFDM, which as discussed above is a very important requirement in a cognitive radio network, OFDM seems to be the most widely adopted

waveform in most wireless standards. For example, OFDM is chosen as the primary transmission in the 3rd Generation Partnership Project (3GPP) LTE [10], WiFi [11], WiMAX [12] and most importantly in the two recent cognitive radio standards IEEE 802.22 WRAN [13] and IEEE 802.11af [14, 15]. It has also been adopted in broadcasting systems such as Digital Video Broadcasting (DVB) [16] and Digital Audio Broadcasting (DAB) [17]. This prevalent adoption of OFDM is mainly due to the numerous advantages it offers compared to other multicarrier waveforms. For example, OFDM can effectively handle the performance deterioration imposed by frequency selective channels by dividing the transmission bandwidth into smaller, low rate frequency bands [18], that operate under flat fading conditions, thereby allowing the use of simple single tap equalizers for data recovery. Furthermore, it is capable of reducing the effects of inter-symbol interference (ISI) introduced by the channel delay spread. ISI happens when adjacent OFDM symbols leak into each other. By adding a guard interval longer than the channel delay spread between adjacent symbols, OFDM can completely eliminate the effects of ISI. This guard interval is known as the cyclic prefix (CP) and is constructed by copying the last samples of the OFDM symbol and appending them to the start of the symbol. Due to all of these factors and its waveform agility, OFDM seems to be a natural choice for cognitive radio [19].

Despite all the attractive features outlined above, OFDM suffers from two major drawbacks: 1) high OOB power leakage and 2) high peak-to-average power ratio (PAPR). Both of these shortcomings have a large impact on the performance of OFDM and can greatly limit its adoption in a cognitive radio network, as they both contribute to the interference created by the OFDM waveform. The focus of this dissertation is to address these two problems in order to minimize the interference and enable coexistence between SU and PU users in the cognitive radio network.

1.2 Dissertation Objectives

As mentioned in the previous discussion, classical OFDM typically does not meet the spectral emission requirements of cognitive radio standards, as well as many other wireless standards. The prime reason that OFDM signals have high spectral emissions outside the designated transmission band is due to the finite duration of the rectangular pulse typically used in the construction

of OFDM signals. Rectangular pulses have a *sinc* like shape in the frequency domain, which causes the OFDM spectrum to decay slowly as f^{-2} [20]. Such slow decaying can potentially create severe interference to users operating in adjacent frequency bands [21]. As a result of the high OOB emissions, the transmission channels in an OFDM system are typically spaced further apart in order to reduce the impact of the resulting interference on adjacent channels. This results in a waste of spectrum and reduces the overall spectral efficiency of the system. Thus, reducing the OOB emissions of OFDM ultimately leads to an improvement of the system spectral efficiency, as transmission channels can be placed closer to each other.

In addition to the high OOB emissions, OFDM also has a high PAPR problem. The PAPR problem arises from the fact that OFDM signals are composed of multiple subcarriers with independent amplitudes and phases, that when added together, are more likely to generate a signal with high peak power [22]. Such peak power may lead to the signal being severely clipped, especially if it exceeds the linear region of operation of the transmitter power amplifier (PA). Signal clipping creates serious inband distortion that ultimately results in large degradation in the bit error rate (BER) performance at the receiver. Besides the inband distortion, high PAPR increases the OOB emissions which is known as a spectral regrowth problem [23]. Thus, the high PAPR characteristic of OFDM indirectly creates interference that can potentially harm users in adjacent channels.

For the reasons outlined in the discussion above, the objective of this dissertation is to develop PHY layer solutions to reduce the interference as a result of the high OOB emissions and PAPR associated with OFDM signals. Typically, reducing the interference in OFDM systems entails trading off either the spectral efficiency or the error rate performance. However, and as discussed before, next generation networks, such as 5G, require very high spectral efficiency in order to meet the increasing demand in broadband services. Accordingly, our focus in this dissertation is the development of algorithms that reduce the interference while maintaining the spectral efficiency of classical OFDM. We also target solutions that result in an error performance identical or close to that of classical OFDM.

1.3 Contributions

1.3.1 Mask Compliant Precoder

In Chapter (3), we propose a precoder for shaping the spectrum of orthogonal frequency division multiplexing (OFDM) signals. Unlike existing methods that focus on minimizing or forcing the spectral sidelobes to zero, the proposed precoder is designed with the goal of controlling the out-of-band emissions beneath a particular power level without impacting the bit error rate (BER) performance. A small distortion is added to the information symbols forcing the emitted spectrum under a prescribed radio frequency mask. Obtained results show that the BER performance of the proposed precoder is similar to that of uncoded OFDM under relaxed masks. We also investigated the impact of the proposed precoder on edge subcarriers. Error vector magnitude (EVM) per subcarrier shows the designed precoder introduces more distortion on edge subcarriers. Consequently, the proposed precoder when combined with adaptive modulation provides further improvement in BER performance under strict masks.

1.3.2 Suppressing Alignment: Joint PAPR and Out-of-Band Power Leakage Reduction for OFDM-Based Systems

In Chapter (4), we propose a novel approach called *suppressing alignment* for the joint reduction of the OOB power leakage and PAPR. The proposed approach exploits the temporal degrees of freedom provided by the CP, a necessary redundancy in OFDM systems, to generate a suppressing signal, that when added to the OFDM symbol, results in marked reduction in both the OOB power leakage and PAPR. Additionally, and in order to not cause any interference to the information data carried by the OFDM symbol, the proposed approach utilizes the wireless channel to perfectly align the suppressing signal with the CP duration at the OFDM receiver. In doing so, we essentially maintain a BER performance similar to legacy OFDM without requiring any change in the receiver structure. To the best of our knowledge, this the first scheme that exploits the degrees of freedom provided by the CP and the wireless channel for spectral emissions reduction without degrading the error performance or reducing the spectral efficiency.

1.3.3 Two Error Vector Magnitude Compliant Precoders for Out-of-Band Power Leakage Reduction in OFDM Based Systems

In Chapter (5), we consider linear precoding as a mean of reducing the spectral emissions of Orthogonal Frequency Division Multiplexing (OFDM). However, we focus on the design of linear precoders in a transparent manner, where the receiver does not need to know the precoding done at the transmitter, thereby eliminating the need to transmit any side information to the receiver or introducing any changes in the legacy OFDM receiver structure. To this end, we utilize the degrees of freedom provided by the Error Vector Magnitude (EVM) tolerance. We first present a closed-form full rate precoder capable of achieving remarkable OOB power leakage reduction while limiting the distortion introduced on the transmitted signal to EVM values specified by the OFDM standard. Second, we present a different precoder with better spectral suppression, albeit at a slightly reduced transmission rate, that produces transmitted signals with similar EVM values to those specified in the standard. Although the second precoder does not have a close-form expression, it can be computed numerically off-line, and only once for a given spctral occupancy.

CHAPTER 2

SURVEY

2.1 Introduction

The goal in this chapter is to provide a comprehensive review of the main OOB power leakage reduction algorithms. The chapter also provides a unified framework under which most of the out-of-band radiation reduction algorithms can be described. The chapter is organized as follows: Section 2.2 gives the system model under which various OOB power leakage reduction algorithms are described. Section 2.3 presents the most important metrics considered in evaluating the performance of OOB power leakage reduction algorithms. In Section 2.4, we present a review of the most important algorithms for the reduction of OOB power emissions. Future directions are given in Section 2.5. Finally, our conclusion is given in Section 2.6.

2.2 OFDM System Model for Out-of-band Power Leakage Reduction

To describe the out-of-band reduction schemes, a matrix based framework is introduced below. The time domain OFDM symbol can be written as

$$\mathbf{s} = \mathbf{P}_{\mathrm{T}}\mathbf{C}_{\mathrm{cp}}\mathbf{Q}^{\mathrm{H}}\mathbf{P}_{\mathrm{F}}\mathbf{d} \tag{2.1}$$

where the vector $\mathbf{d} \in \mathbb{C}^{N\times 1}$ contains the information data to be transmitted, $\mathbf{P}_{\mathrm{F}}$ denotes a linear transformation matrix in the frequency domain, $\mathbf{Q}$ is the fast Fourier transformation (FFT) matrix. $\mathbf{P}_{\mathrm{T}}$ is a linear transformation matrix in the time domain. The matrix $\mathbf{C_{cp}}$ adds a CP of length L to the beginning of every OFDM symbol and is defined in (2.2) below. We will follow this framework throughout the chapter to explain most sidelobe suppression methods. The processing

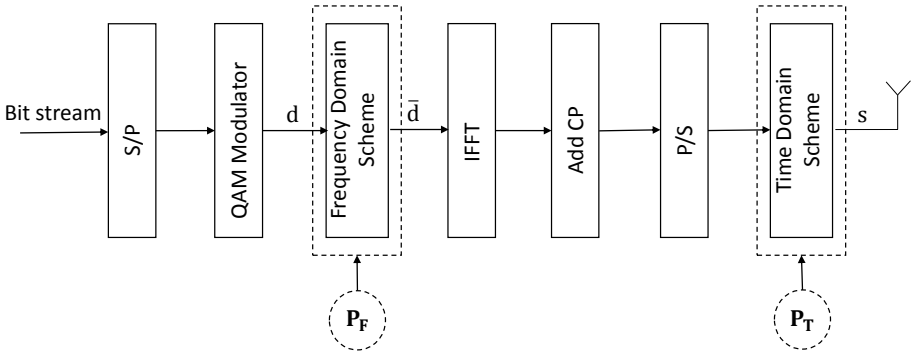

Figure 2.1 System model OFDM with OOB power leakage reduction.

matrices $\mathbf{P}_{\mathrm{T}}$ and $\mathbf{P}_{\mathrm{F}}$ describe the additional processing blocks introduced in the OFDM transmitter as shown in Figure 2.1 for the purpose of reducing the OOB emissions, and will be referred to as precoding or transformation matrices interchangeably from now on. Note that if both $\mathbf{P}_{\mathrm{T}}$ and $\mathbf{P}_{\mathrm{F}}$ are the identity matrix, $\mathbf{s}$ represents just plain OFDM samples. Moreover, if we are describing a time domain method such as windowing, $\mathbf{P}_{\mathrm{T}}$ would be a diagonal matrix containing the samples of the window function and $\mathbf{P}_{\mathrm{F}}$ would be the identity matrix. In general, $\mathbf{P}_{\mathrm{F}}$ would be the identity matrix if we are describing a time domain scheme, and $\mathbf{P}_{\mathrm{T}}$ would be the identity matrix if we are describing a frequency domain scheme.

$$\mathbf{C}_{\mathrm{cp}} = \begin{bmatrix} \mathbf{0}_{L\times(N-L)} & \mathbf{I}_L \\ & \mathbf{I}_N \end{bmatrix} \tag{2.2}$$

We also define the interference coefficient matrix $\mathbf{A}$ that hold the leakage contribution of every subcarrier in the out-of-band region as follows: let $a_k(f)$ be the interference coefficient from the kth subcarrier to any frequency f in the out-of-band region, which can be obtained by the taking the Fourier transform of the rectangularly windowed kth subcarrier

$$a_k(f) = \int_{-\frac{T}{2}}^{\frac{T}{2}} e^{\frac{j2\pi k}{T_s}t} e^{-j2\pi ft} dt = \mathrm{sinc}\left(T(f - \frac{k}{T_s})\right) \tag{2.3}$$

where T is the length of the OFDM symbol. The interference coefficient matrix $\mathbf{A}$ is then defined as

$$[\mathbf{A}]_{m,k} = a_k(f_m) \tag{2.4}$$

where f_m is any frequency outside the transmission band. This interference coefficient matrix will be used throughout the chapter to aid in the description of the various out-of-band reduction algorithms.

2.3 Performance Metrics for Out-of-band Emission Reduction Algorithms

2.3.1 Power Spectral Density and Adjacent Channel Leakage Ratio

The power spectral density (PSD) and the adjacent channel leakage ratio (ACLR) are the two most used figures of merit for the measurement of out-of-band emissions. The PSD shows the spectral emissions of the radio transmitter across the frequency band. It is used mostly in determining whether the out-of-band power from wireless devices complies with the radio frequency (RF) emissions set by regulatory agencies. Power emissions of all wireless devices have to usually fall inside a strict SEM specified by regulatory entities such as the FCC in the United States and Office of Communications (Ofcom) in the United Kingdom. While the power spectral density measures the power emissions of the transmitter, the ACLR on the other hand estimates how much power is leaked into the adjacent channel, thereby showing the effect of the transmitter power emissions on nearby devices.

2.3.2 Bit Error Rate

Although the performance of out-of-band interference reduction schemes is usually quantified by the PSD or ACLR, another equally important metric is the BER. This is because for most schemes, while their main goal is to reduce the out-of-band emissions, they do so by sacrificing the error performance. For example, some schemes reserve some subcarriers for the sole purpose of minimizing the spectral emissions. This effectively reduces the useful signal-to-noise ratio (SNR) as

these subcarriers do not carry any information, leading to degradation in the BER. Other schemes reduce the out-of-band emissions by distorting the data symbols, and depending on how large this distortion is, the BER performance will be affected accordingly. The trade-off between the out-of-band interference reduction and BER performance is very evident is most of the proposed algorithms.

2.3.3 Data Rate Loss

Just as there is a trade-off between the out-of-band interference reduction and the BER, there is also a trade-off with the spectral efficiency. As mentioned before, some of the spectral suppression algorithms reserve some subcarriers for the sole purpose of reducing the emissions. The data rate loss comes from the fact that these subcarriers carry non-information data which might have otherwise been used for data transmission. Other schemes extend the OFDM symbol in time, therefore decreasing the throughput. The ultimate goal of most techniques is to have a balance between the amount of interference reduction and data rate loss.

2.3.4 Peak-to-Average Power Ratio

The PAPR is a very important performance metric for OFDM waveforms and is defined as the ratio of the peak instantaneous power to the average power of the transmitted signal. Multi-carrier waveforms, including OFDM are known to have high PAPR. This is due to the fact that OFDM signals are composed of independent data modulated over multiple subcarriers that might add up coherently, therefore creating large peaks while the average power stays relatively the same. High PAPR requires the power amplifier of the transmitter to have a large dynamic range, otherwise the signal will be clipped creating what is known as the spectral regrowth problem, where the sidelobes of the signal would grow back up, even after being suppressed before the power amplifier. Therefore it is necessary that algorithms developed for suppressing the spectral sidelobes of OFDM do so without increasing the PAPR of the transmitted signal.

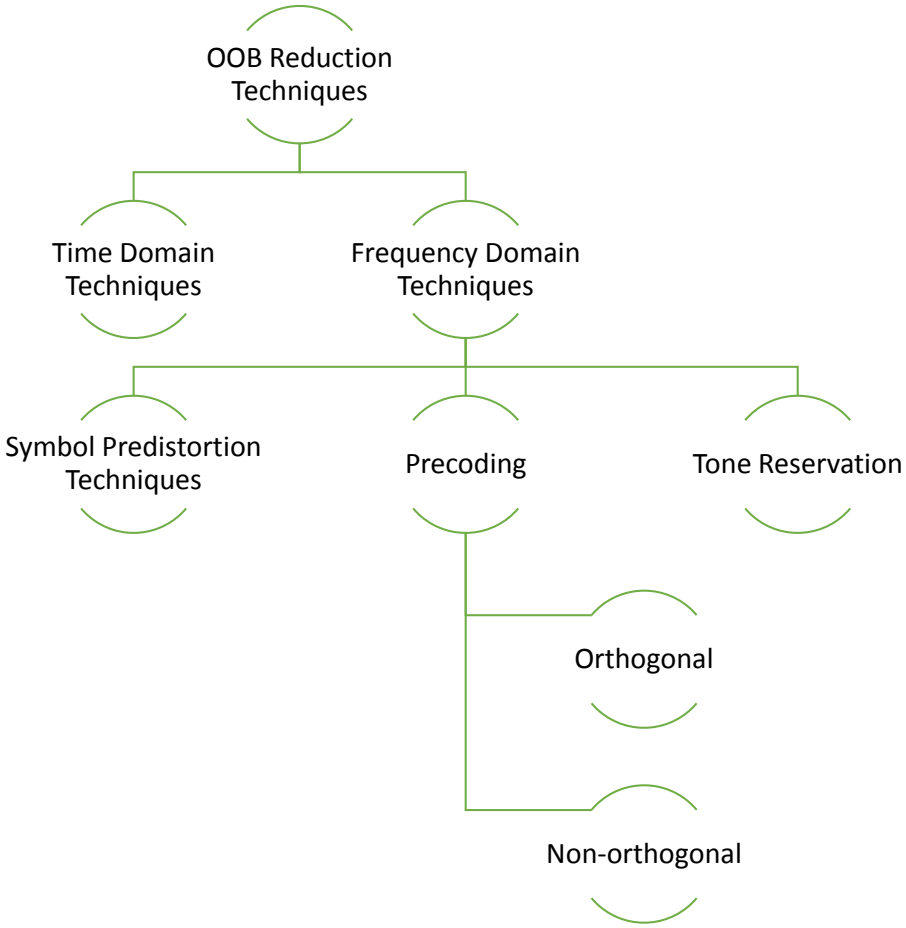

Figure 2.2 Classification of OOB power leakage reduction algorithms.

2.3.5 Computational Complexity

Wireless devices have limited processing power and memory, therefore developing algorithms that match the processing power of these devices is of paramount importance. Most of the techniques that achieve remarkable spectral suppression, have prohibitive computational complexity which imposes significant delays and additional processing power that makes them unrealizable in real time applications.

2.4 OOB Reduction Techniques

The out-of-band leakage in OFDM is large enough to cause severe interference in neighboring channels. This is very critical, especially in cognitive radio applications where SU users are not allowed to cause any interference to PU users. While simply turning off subcarriers close to the band edges slightly reduces the out-of-band leakage, this reduction is not sufficient to allow operation in neighboring channels, since the sidelobes decay very slowly, asymptotically as f^{-2} [20]. As a result, many methods were developed for reducing the spectral emissions in OFDM. Most of these methods can be classified under two main categories: frequency domain techniques and time domain techniques with the frequency domain category subdivided further in several subcategories as shown in Figure 2.2. In this section, some of the most well known methods in each category will be discussed.

2.4.1 Frequency Domain Techniques

Frequency domain algorithms typically reduce the OOB emissions of OFDM by operating on the incoming data in the frequency domain through some transformation matrix $\mathbf{P}_{\mathrm{F}}$ as shown in Figure 2.1. Frequency domain algorithms can be classified under three main subcategories: precoding schemes, tone reservation schemes and symbol predistortion techniques as shown in Figure 2.2. We will discuss most of the algorithms under each subcategory, but first we will give some background on the properties of the transformation matrix $\mathbf{P}_{\mathrm{F}}$ that will help in understanding most of the frequency domain algorithms, particularly precoding algorithms.

The transformation $\mathbf{P}_{\mathrm{F}}$ is considered orthogonal if its columns are drawn from an orthogonal basis. Put differently, any transformation $\mathbf{P}$ that satisfies $\mathbf{P}^{\mathrm{H}}\mathbf{P} = \mathbf{I}$ is an orthogonal transformation. This is a necessary and sufficient condition for the transformation to be orthogonal. Additionally, if the transformation satisfies $\mathbf{P}\mathbf{P}^{\mathrm{H}} = \mathbf{I}$, it is considered a *square* orthogonal transformation. Orthogonal transformations are desirable in the sense that they preserve the orthogonality among the subcarriers in OFDM as opposed to non-orthogonal transformations which destroy the orthogonality between the subcarriers and degrade the error performance. This is true regardless of whether the transformation is square or rectangular. Additionally, a *square* orthogonal transformation, by

virtue of being a complete matrix, does not reduce the transmission rate of the system compared to rectangular orthogonal transformations. However, square orthogonal transformations are not capable of reducing the out-of-band power leakage. Therefore, in order to reduce the OOB emissions of OFDM while maintaining the orthogonality between the subcarriers, $\mathbf{P}_{\mathrm{F}}$ has to be a rectangular orthogonal matrix. $\mathbf{P}_{\mathrm{F}}$ can be designed to be a full matrix to maintain the transmission rate, but it cannot be orthogonal is such a case if the purpose of the design is to reduce the OOB emissions. This shows the trade-off between the error rate and the data rate that we will encounter in most of the out-of-band reduction algorithms.

Most frequency domain techniques, especially precoding algorithms, reduce the the out-of-band emissions in OFDM by introducing correlation between the modulated symbols. According to [24], the OFDM power spectrum is

$$P(f) = \frac{1}{T}\mathbf{a}^{T}(f)E\{\mathbf{d}\mathbf{d}^{\mathrm{H}}\}\mathbf{a}^{*}(f) \tag{2.5}$$

where T is the length of the OFDM symbol, $\mathbf{a}(f)$ is a vector with elements defined in (2.3), $(.)^{T}$ is the transpose and $(.)^{*}$ is the conjugate operator. The result in (2.5) clearly shows the impact of the correlation between the modulated data within one OFDM symbol on the power spectrum. The modulated data are usually assumed to be uncorrelated, i.e, $E\{\mathbf{d}\mathbf{d}^{\mathrm{H}}\} = \mathbf{I}$, therefore the power spectrum becomes

$$P(f) = \frac{1}{T}\mathbf{a}^{\mathrm{T}}(f)\mathbf{a}^{*}(f) = \frac{1}{T}\|\mathbf{a}(f)\|_{2}^{2} \tag{2.6}$$

which is the sum of the power of the sinc functions, i.e, the power spectrum of plain OFDM waveforms. Therefore, in order to reduce the OOB power leakage, most of the precoding algorithms discussed below have transformation matrices $\mathbf{P}_{\mathrm{F}}$ that introduce correlation between the modulated symbols.

2.4.1.1 Precoding Techniques

The concept of precoding has been exploited extensively in the past to improve various performance characteristics of OFDM. For example, in [25] precoding is used for reducing the PAPR and in [26, 27] it is used to counteract the effects of the channel and improve the error performance. Recently precoding has been explored for the purpose of reducing the out-of-band emissions in OFDM [1, 28–38]. The main idea, as mentioned in the previous discussion, is to introduce correlation between the transmitted data stream using some transformation $\mathbf{P}_{\mathrm{F}}$ in order to produce new data symbols with better spectral emissions. Most sidelobe suppression schemes that operate directly on the data, i.e., frequency domain algorithms, fall under the precoding category. However, for the purpose of this review the term precoding refers to only those methods whose precoding or transformation matrix is independent of the data stream, i.e., the transformation matrix is fixed and does not have to be computed for every incoming OFDM symbol. There are various types of precoding schemes designed under different conditions and criteria, but all with the one goal of reducing the out-of-band emissions. These precoding methods will be discussed below.

2.4.1.1.1 Non-orthogonal Precoding

Non-orthogonal precoders are full rate precoders in the sense that they do not reduce the transmission rate of the data stream. They achieve spectral suppression by introducing correlation among the modulated data within one OFDM symbol, just like all other frequency domain precoders (orthogonal or not orthogonal). However, they do so by sacrificing the error performance, since the orthogonality of the transmission scheme is destroyed by the precoding operation. One example of such precoders is the precoder presented in [1]. It achieves remarkable spectral suppression by projecting the modulated data into the nullspace of the interference coefficient matrix defined in (2.4). The nullspace of any matrix $\mathbf{B}$ is all vectors $\mathbf{x}$ such that $\mathbf{Bx} = \mathbf{0}$. Therefore by mapping the original modulated symbols $\mathbf{d}$ to a new set of symbols $\bar{\mathbf{d}}$ using a linear transformation such that $\bar{\mathbf{d}}$ lies completely in the nullspace of $\mathbf{A}$, the OOB power leakage at some selected frequencies (frequencies defined in $\mathbf{A}$) can be completely eliminated. Moreover, $\bar{\mathbf{d}}$ is found by orthogonally projecting

the data vector $\mathbf{d}$, which provides the nearest vector to $\mathbf{d}$, thereby providing the minimum error probablity among all nullspace vectors. Using the framework defined in (2.1) with $\mathbf{P}_{\mathrm{T}} = \mathbf{I}$ and $\mathbf{P}_{\mathrm{F}}$ is the nullspace orthogonal projection transformation defined as (see [39] for more information about projections)

$$\mathbf{P}_{\mathrm{F}} = \mathbf{I} - \mathbf{A}^{\mathrm{H}}(\mathbf{A}\mathbf{A}^{\mathrm{H}})^{-1}\mathbf{A} \ . \tag{2.7}$$

Precoding the information symbols with this projection matrix nulls the sidelobes at the set of discrete frequencies defined in $\mathbf{A}$. However, the objective is to zero all power leakage in the OOB, not just at a number of discrete frequency locations. Fortunately, the results in [1] show that through careful selection of the discrete frequency set where the nulls are placed, the whole out-of-band spectrum can be significantly minimized. It was shown that by selecting pairs of notching frequencies next to each other, the spectrum at these frequencies as well as the surrounding frequencies will be suppressed.

The nullspace projection precoder in [1] achieves remarkable sidelobe suppression compared to other algorithms. However, it does so at the expense of a significant reduction in the error performance. This so because by virtue of being a projection precoder, the precoder in [1] maps the data vector from a higher dimensional subspace to a lower dimensional subspace, effectively reducing its distance properties. The interference coefficient matrix $\mathbf{A} \in \mathbb{C}^{\mathbb{M}\times\mathbb{N}}$, where M is the number of frequencies where the sidelobe nulls are placed and N is the total number of subcarriers, has a nullspace with a dimension of $N - M$. Therefore, the precoder in (2.7) where $\mathbf{P}_{\mathrm{F}}$ is $N \times N$, projects the data from an N-dimensional subspace onto the $(N - M)$ dimensional nullspace of the interference matrix, thereby distorting the data. Another interpretation of the reduction in the error performance of the precoder (2.7) is that projections are generally non-invertible, so once the data is distorted by projection, that distortion is irreversible. This also explains the reduction in error performance even if the receiver knows the projection operation done at the transmitter. A different non-orthogonal precoder that also projects the transmitted data into the nullspace of the OOB interference matrix is presented in [28]. It has a precoding matrix similar

to (2.7). The difference here is that not all subcarriers are utilized for data transmission, some subcarriers are reserved to mitigate the distortion introduced by the projection precoder and aide in the data recovery at the receiver. However, its error performance is still inferior to plain OFDM. Additionally, it reduces the transmission rate due to the use of the reserved subcarriers that do not carry any information data. Another non-orthogonal precoder was presented in [33] that achieves spectral sidelobes decaying as $f^{-2(L+1)}$, where L is a design parameter, however it suffers from the same error performance that is generally associated with non-orthogonal precoders.

A novel non-orthogonal precoder called N-continuous OFDM [31] that recognizes the signal discontinuity as the main cause of the high OOB power leakage in OFDM. Making the OFDM symbols continuous at the symbol edges leads to smoother transitions between consecutive symbols and effectively reduces the OOB emissions. Continuity and smoothness are related to the number of continuous derivatives, therefore smooth transitions can be created by making the transmitted signal and its first N derivatives continuous at the symbol borders by satisfying

$$\frac{d^n}{dt^n} s_i(t)|_{t=-T_g} = \frac{d^n}{dt^n} s_{i-1}(t)_{t=T_s} \tag{2.8}$$

where T_g is the CP duration and T_s is the useful symbol duration. The formulation in (2.8) makes the current OFDM symbol as well as its first N derivatives at $t = -T_g$ (start of the symbol) equal to those of the previous symbol at $t = T_s$ (end of the symbol). Signals satisfying (2.8) are said to be N-continuous and have smooth transitions at the symbol edges. The path towards generating smooth signals here differs greatly from the one followed in time-domain windowing (discussed below). In the windowing method, the time-domain OFDM symbol is extended in time as well as scaled down at the symbol edges by the window function. This process contaminates the CP, effectively reducing its size. To overcome such a shortcoming, N-continuous OFDM modifies the original information data directly in the frequency domain. The authors proposed to precode the data stream $\mathbf{d}_i$ of the current OFDM symbol to generate new symbols $\bar{\mathbf{d}}_i$ the satisfy the N-continuity criteria above. Achieving signal continuity in this manner requires information about the previous symbol which might create some memory and buffering constraints on the transmitter. To alleviate

those problem, a memoryless precoder that achieve the signal continuity is reported in [2] where the derivatives at the two edges of the time domain OFDM symbol are forced to zero. This way, every OFDM symbol as well as its derivatives start and end at zero which makes consecutive symbols continuous and is accomplished by

$$\frac{d^n}{dt^n} s_i(t)|_{t=-T_g} = \frac{d^n}{dt^n} s_i(t)_{t=T_s} = 0 \ . \tag{2.9}$$

The linear constraints represented (2.9) are collected in some matrix $\mathbf{B}$ and the information vector $\mathbf{d}$ is projected into its nullspace using the precoder $\mathbf{P}_{\mathrm{F}}$. The design of the precoder $\mathbf{P}_{\mathrm{F}}$ is similar to (2.7), the only difference here is that subspace where the information data is projected to is represented by some matrix $\mathbf{B}$ that hold the continuity conditions in (2.9). Just as the case with all projection precoders where the data is mapped to a smaller subspace, the N-continuous OFDM precoder in [2] degrades the BER performance compared to that of plain OFDM. N-continuous OFDM improves the spectral containment of OFDM significantly with even deeper spectral suppression as the order of continuity N increases. However, the BER performance deteriorates as the order of continuity increases. To improve the BER performance, an N-continuous OFDM precoder that maintains the orthogonality between the subcarriers is presented in [32]. This precoder provides similar BER performance as classical OFDM; however it does so by trading off the data rate. Moreover, it requires the previous OFDM symbol in order to achieve continuity, which puts extra requirements on the transmitter in terms of memory resources. While the precoders in [2, 31, 32] are fixed and need to be computed once, they have prohibitive computational complexity that increases with the number of subcarriers which makes their implementation in practice not feasible.

2.4.1.1.2 Orthogonal Precoding

Orthogonal precoders maitain the same error performance as uncoded OFDM. However, using orthogonal precoders to suppress the sidelobes usually comes at the expense of some reduction in the data rate. The precoders discussed in this subsection are usually designed to achieve similar spectral suppression performance as non-orthogonal precoders, albeit at a lower transmission rate,

while preserving the orthogonality among the subcarriers and producing waveforms with error performance similar to OFDM. In [29], the data stream is mapped using a linear transformation $\mathbf{P}_{\mathrm{F}}$ such that it lies completely in the nullspace of the interference coefficient matrix $\mathbf{A}$. However, this time, the mapping is restricted to being an orthogonal multiplexing mapping, i.e, the columns of the linear transformation $\mathbf{P}_{\mathrm{F}}$ are constructed from an orthonormal basis set. In this particular case, the basis set is chosen to be the orthonormal basis for the nullspace of the interference coefficient matrix $\mathbf{A}$. Since any linear combination of the nullspace basis remains in the nullspace, this ensures that the precoded data $\bar{\mathbf{d}} = \mathbf{P}_{\mathrm{F}}\mathbf{d}$ reside completely in the nullspace, therefore nulling the spectrum at the discrete frequencies defined in $\mathbf{A}$ and reducing the spectrum at the surrounding frequencies as well. However, the nullspace of the interference matrix $\mathbf{A}$ has only $N-M$ dimensions, where N is the number of subcarriers and M is the number of notched frequencies. Therefore, its nullspace has only $N-M$ orthogonal basis. Consequently, the orthogonal precoder $\mathbf{P}_{\mathrm{F}}$ which has its columns composed of these basis, can only multiplex $N-M$ data symbols, effectively reducing the transmission rate of the system (only $N-M$ of N subcarriers carry information data). As we mentioned before, orthogonal transformations cannot reduce the spectral emissions without trading off the transmission rate of the system. Furthermore, it is very complex and unrealizable in practice, especially for a system with a large number of subcarriers.

In [30], it was shown that the total average power of the out-of-band leakage is the sum of the singular values of the interference coefficients matrix $\mathbf{A}$. An orthogonal precoder was designed that blanks out the largest singular values, therefore reducing the power leakage. This precoder converges to the one in [29] discussed above if all singular values are zeroed by the precoder, effectively forcing the signal to the nullspace. Several other orthogonal precoders were proposed in [34].

Frequency domain orthogonal precoders achieve huge reduction in the out-of-band leakage and provide similar error performance to OFDM, however, as stated above, their computational complexity is not tractable for real time applications. Furthermore, they are not spectrally efficient, especially for cognitive radio scenarios where the frequency holes are narrowband and scattered across the spectrum.

2.4.1.2 Data Adjusting Techniques

Data adjusting schemes are similar to the frequency domain precoding schemes discussed above, where the spectral suppression is achieved by directly modifying the information data in the frequency domain. However, for the precoding schemes, the transformation or precoding matrix is fixed. Here the precoder is not fixed and has to be computed for every OFDM symbol. As a result, most data adjusting schemes have high computational complexity.

A widely known data adjusting scheme is subcarrier weighting [40, 41], where all subcarriers are multiplied with real-valued weights with the goal of minimizing the sidelobes in the OOB region. This can be realized by designing $\mathbf{P}_{\mathrm{F}}$ in (2.1) as a diagonal precoding matrix of the form:

$$\mathbf{P}_{\mathrm{F}} = \begin{bmatrix} p_1 & 0 & \dots & 0 \\ 0 & p_2 & \dots & 0 \\ \vdots & \vdots \ddots & \vdots & \\ 0 & 0 & \dots & p_N \end{bmatrix} , \tag{2.10}$$

where the optimal weights p_i are determined by minimizing the OOB power of the weighted OFDM signal according to

$$\mathbf{P}_{\mathrm{F}} = \arg\min_{\mathrm{P_F}} \| \mathbf{A} \underbrace{\mathbf{P}_{\mathrm{F}} \mathbf{d}}_{\bar{\mathbf{d}}} \|_2^2 , \tag{2.11}$$

where $\mathbf{A}$ is interference coefficient matrix defined in (2.4), and $\bar{\mathbf{d}}$ are a new set of symbols generated by the precoding matrix $\mathbf{P}_{\mathrm{F}}$ with better spectral emissions compared to the original symbols $\mathbf{d}$. In order to guarantee that the new symbols have the same power as the original data, the following constraint is introduced to the optimization problem in (2.11)

$$\|\bar{\mathbf{d}}\|_2^2 = \|\mathbf{d}\|_2^2 . \tag{2.12}$$

Since the original data has been modified by the precoding matrix $\mathbf{P}_{\mathrm{F}}$, the receiver needs to know $\mathbf{P}_{\mathrm{F}}$ to be able to recover the original data. This entails transmitting a large amount of side information

to the receiver which leads to huge reduction in the data rate. To alleviate such a problem, the weights of the precoding matrix $\mathbf{P}_{\mathrm{F}}$ are designed in such a way that the new symbols $\bar{\mathbf{d}}$ remain in the same decision region as the original symbols. This way the generated symbols $\bar{\mathbf{d}}$ can be detected without the need for any side information to be transmitted to the receiver. To achieve this, the weighting coefficients in (2.10) have to be real and lie between predefined limits, which leads to the second constraint

$$p_{\min} \leq p_i \leq p_{\max} \ . \tag{2.13}$$

The optimization problem in (2.11) along with the two constraints in (2.12) and (2.13) is a non-linear programming problem with a quadratic equality and a linear inequality constraints. Its solution leads to the precoding matrix $\mathbf{P}_{\mathrm{F}}$ that is used to process the information data and produce new transmitted symbols with better spectral emissions.

One of the disadvantages of the subcarrier weighting scheme is the increased computational complexity incurred on the transmitter, as the precoding matrix $\mathbf{P}_{\mathrm{F}}$ has to be computed for every OFDM symbol. Another drawback stems from the fact that after multiplication with the precoding matrix $\mathbf{P}_{\mathrm{F}}$, each subcarrier will have a different amount of power compared to other subcarriers because of the different weights of the diagonal matrix $\mathbf{P}_{\mathrm{F}}$. This unequal transmit power on all subcarriers leads to degradation in the BER performance, especially in frequency selective channels. To overcome the impact of the channel selectivity, OFDM signals typically adapt the subcarrier parameters such as the choice of the modulation scheme and subcarrier power. This is referred to as bit-power loading, where the total throughput can be maximized by loading subcarriers that experience low SNR with symbols drawn from a low modulation order, while allocating more power to those subcarriers that have high SNR. To suppress the spectral sidelobes, the subcarrier weighting scheme changes the power on each subcarrier. This fact leads to a conflict between the spectral sidelobe suppression achieved by subcarrier weighting and the capacity maximization due to the bit-power loading algorithm. A solution to this problem is proposed in [42], where the

sidelobe suppression problem is viewed as a capacity maximization problem subject to a power leakage interference constraint.

2.4.1.3 Tone Reservation Techniques

Tone reservation techniques are based on the concept of allocating or reserving some subcarriers that are modulated with weighting coefficients calculated in such a way that the total OOB power leakage is reduced. The weighting coefficients on these subcarriers are calculated based on either a frequency domain criterion or a time domain criterion. Depending on which criterion is employed, the location of the reserved subcarriers can be at the edges of the spectrum or spread throughout the whole spectrum. It should be stressed here that the reserved subcarriers can be anywhere in the spectrum. They do not have to necessarily be at the edges, which is a misconception as the concept of reserved tones is usually confused with the idea of cancellation carriers; a scheme that falls under the reserved tones techniques which will be discussed below. The idea of tone reservation is not new and has long been used before for the purpose of PAPR reduction [43] [44].

2.4.1.3.1 Cancellation Carriers

In the cancellation carriers scheme [45, 46], the reserved tones or so called cancellation carriers (CC) are located at the edges on both sides of the OFDM spectrum. These subcarriers do not carry any data information and are modulated with complex weights. The weights are calculated such that the sidelobes resulting from the cancellation carriers cancel or minimize the sidelobes of the transmitted data. This same idea has been proposed before in [47], where the reserved tones are referred to as dummy tones. The only difference is that the weights on the dummy tones are restricted to only be a weighted sum of the data on the other subcarriers.

To describe the cancellation carriers scheme we follow the same framework in (2.1). Since the processing in this case is done in the frequency domain, $\mathbf{P}_{\mathrm{T}}$ is set to the identity matrix. We also assume that there is a mapping $\mathbf{d} \rightarrow \bar{\mathbf{d}}$. However since the cancellation carriers are located at the edges of the spectrum, this mapping affects only the outer data in the vector $\mathbf{d}$ and leaves the

inner data intact. The mapped vector $\bar{\mathbf{d}}$ is written as

$$\bar{\mathbf{d}} = \begin{bmatrix} p_1 & 0 & \dots & \dots & \dots & 0 & 0 \\ 0 & p_2 & \dots & \dots & \dots & 0 & 0 \\ \vdots & \vdots & \mathbf{I}_{1,1} & & & \vdots & \vdots \\ \vdots & \vdots & & \ddots & & \vdots & \vdots \\ \vdots & \vdots & & & \mathbf{I}_{N,N} & \vdots & \vdots \\ 0 & 0 & \dots & \dots & \dots & p_3 & 0 \\ 0 & 0 & \dots & \dots & \dots & 0 & p_4 \end{bmatrix} \begin{bmatrix} 1 \\ 1 \\ d_1 \\ \vdots \\ d_N \\ 1 \\ 1 \end{bmatrix} \tag{2.14}$$

where $\mathbf{I}$ is the identity matrix. In this example, only four cancellation carriers are used, two on each side of the spectrum. The spectral leakage power resulting from the new vector $\bar{\mathbf{d}}$ is

$$\mathbf{C} = \|\mathbf{A}\mathbf{P}_{\mathrm{F}}\mathbf{d}\|^2 \tag{2.15}$$

where $\mathbf{A}$ holds the interference from every modulated subcarrier in the out-of-band region and is defined in (2.4). As stated before, the weights p_i are calculated such that the power leakage is minimized. Therefore, the precoding matrix $\mathbf{P}_{\mathrm{F}}$ is found according to

$$\mathbf{P}_{\mathrm{F}} = \arg\min_{\mathrm{P_F}} \|\mathbf{A}\mathbf{P}_{\mathrm{F}}\mathbf{d}\|^2 \tag{2.16}$$

Due to the limited transmission power for every OFDM symbol, and since the cancellation carriers do not carry any data information, the power on these subcarriers is usually bounded below some defined value. This leads to the following constraint

$$\|\mathbf{P}\|_2^2 < \alpha \tag{2.17}$$

where $\mathbf{P} = [p_1, p_2, p_3, p_4]^{\mathrm{T}}$ is the vector holding the weights of the cancellation carriers. The optimization problem in (2.16) along with the constraint in (2.17) is known as a linear least squares

problem with a quadratic inequality constraint. Readers interested in the solution of the optimization problem can refer to [45] and the references therein.

The transformation matrix $\mathbf{P}_{\mathrm{F}}$ for the cancellation carriers scheme is similar to that of subcarrier weighting in (2.10). The only difference between the two transformations is that: here the middle part of the precoding matrix is always the identity matrix, signifying the fact that only the outer data is affected by the transformation operation. It is these transformed data on the edges that constitute the cancellation carriers. Also, similar to subcarrier weighting the precoder $\mathbf{P}_{\mathrm{F}}$ is not fixed and have to be updated for every OFDM symbol which adds to the computational complexity of the cancellation carriers scheme. An observation that we would like to make is that the transformation $\mathbf{P}_{\mathrm{F}}$ is an orthogonal transformation which preserves the structure of OFDM. This effectively means that the introduction of cancellation carriers for spectral leakage suppression does not destroy the orthogonality between subcarriers in OFDM. However, while the transformation in (2.14) is an orthogonal transformation, it is not orthonormal i.e., its Frobenius norm is not unity, which is actually part of the reason that it can reduce the spectral leakage power.

Although the orthogonality between subcarriers is preserved by the transformation matrix in cancellation carriers, the fact still remains that these subcarriers take away some power that could have otherwise been used by other subcarriers that carry data information. This effectively reduces the SNR on the data-bearing subcarriers leading to a decreased BER performance. Another drawback of the cancellation carriers scheme is that its suppression performance is week for wider inband spectral gaps [48]. This is mainly because the cancellation carriers are usually located at the band edges, therefore they tend to suppress only those sidelobes closer to edges while the level of suppression decreases as you move way from the edges of the band. This also means that the suppression performance of the cancellation carriers scheme is worse in the far away OOB region [49]. Several algorithms aimed at improving the performance of the cancellation were proposed in [50] and [51]

2.4.1.3.2 Active Interference Cancellation

Conventionally, subcarriers that are located in the transmission band of PU users are usually turned off to minimize the interference to PU users. In active interference cancellation (AIC) schemes [52, 53], these subcarriers are not turned off. Instead, they are active and are calculated in such a way that the total interference in the PU band is canceled. These subcarriers are known as active tones. In addition to the active tones, and just as is done in the cancellation carriers scheme, some subcarriers in the guard bands close to transmission band of PU users are allocated as cancellation carriers. The intention is to have the total sidelobes from the active tones and the cancellation carriers oppose the sidelobes resulting from the data subcarriers, leading to minimal interference in the PU band. In [52], the active tones are placed in locations with the same frequency spacing as the data subcarriers. This is done so that the orthogonality between the active tones and the data subcarriers is maintained and to avoid inter-carrier interference (ICI). To further improve the suppression performance of the AIC scheme in [52], the authors in [53] proposed to place the active tones in locations with smaller frequency spacing than the data subcarriers. However, this breaks the orthogonality between the data subcarriers and the active tones, potentially leading to increased ICI. To limit the effects of the resulting ICI, the authors put a constraint on the interference created by the active tones on the data subcarriers. The sidelobe suppression performance is traded off with the amount of ICI introduced, with more sidelobe suppression achieved if more interference is allowed.

2.4.1.3.3 Time Domain Tone Reservation

Similar to N-continuous OFDM [2, 31], a set of reserved tones in [49] are modulated with complex weights computed in such a way to force N-continuity between consecutive OFDM symbols. The only difference between the two schemes is that in N-continuous, all subcarriers are used force N-continuity, while only a subset of subcarriers are used in this method. Unlike the cancellation carriers scheme, where the subcarriers are clustered around the edges of the transmission band, the reserved tones of this scheme can be located anywhere. This comes as a result of the time domain criterion of forcing continuity, as opposed to the reserved tones in the cancellation carriers scheme

where the objective is for the cancellation carriers to force notches in the spectrum, therefore mandating that they be located at the edges of the band. The proposed method achieves deep sidelobe suppression, however, it suffers from the same drawbacks of the cancellation carriers scheme such as reduced spectral efficiency and high PAPR.

2.4.2 Time Domain Techniques

Perhaps the most known method for reducing the out-of-band interference in OFDM is the time-domain windowing method. The default rectangular window used in OFDM has sharp transitions at the symbol borders. These sharp transitions cause high frequency components in the frequency domain. Therefore, the main objective of time domain windowing is to smooth these transitions by multiplying the OFDM symbol with a window function that scales down the power at the symbol edges. A multitude of window functions can be used for this purpose: hanning, hamming, gaussian, raised cosine, etc. However, our focus here is on window functions that preserve the orthogonality between the OFDM subcarriers. This is achieved by designing window functions such that the useful part of the OFDM symbol, including the CP is not affected or scaled down by the trailing or leading part of the window function. A widely used window function for shaping the spectrum of OFDM signals is the raised cosine window defined in [54] as

$$g(t) = \begin{cases} \frac{1}{2} + \frac{1}{2}\cos(\pi + \frac{\pi t}{\beta T_s}) \ , & 0 \leq t \leq \beta T_s \\ 1 \ , & \beta T_s \leq t \leq T_s \\ \frac{1}{2} + \frac{1}{2}\cos(\frac{\pi (t - T_s)}{\beta T_s}) \ , & T_s \leq t \leq (1+\beta) T_s \end{cases} , \tag{2.18}$$

where β is called the roll-off factor and it is a parameter that controls the decay rate of the window function. Windowing in the context of sidelobe suppression is known as transmit windowing as is usually implemented by introducing an extension of N_w samples at both the beginning and end of the OFDM symbol. The window extensions are then shaped by the window function, which can be any window as long as it preserves the orthogonality between the subcarriers.

Transmit windowing can be interpreted as a kind of time domain precoding, where the precoding or transformation matrix $\mathbf{P}_{\mathrm{T}}$ in (2.1) is a diagonal matrix with the diagonal elements generated by sampling the window function in (2.18). and $\mathbf{P}_{\mathrm{F}} = \mathbf{I}$. The length of the window extensions corresponds to the roll-off factor of the window. More sidelobe suppression is achieved by increasing the length of the window extensions or the roll-off factor. However, this usually comes at the expense of some reduction in the throughput. In general, time domain windowing, while simple and easy to implement, does not achieve sufficient sidelobe suppression unless the throughput is greatly traded-off. Additionally, windowing does not perform well in small inband spectral gaps [48], therefore it, might not generate the level of suppression required for OFDM-based cognitive radio systems.

Similar to the time domain windowing discussed above, the authors in [55] proposed an algorithm that shapes the signal spectrum using an adaptive window function. In the conventional windowing method, the same window function is applied to every OFDM symbol. However, the level of discontinuity or smoothness is different from symbol-to-symbol, i.e., not all symbols have sharp transitions, just as not all of them have smooth transitions. Therefore, using a fixed window for all OFDM symbols might not be optimum in terms of spectral suppression. Recognizing this, an extension is added between every pair of symbols, where the samples of the extension are computed using an optimization algorithm that gives the optimum transition between OFDM symbols. The spectral suppression of this method is superior to that of the conventional windowing method. However, due to the adaptive nature of the algorithm where the window extensions have to be computed for every OFDM symbol, its computational complexity is high which renders it impractical for real time applications. Another improvement over conventional time-domain windowing is proposed in [56]. The proposed method provides an improvement in the spectral efficiency and sidelobe suppression by allowing controllable ISI and ICI between subcarriers. In the conventional windowing method described above, the same window function is applied to all subcarriers, effectively treating the spectral emissions of all subcarriers the same. However, subcarriers at band edges usually create more spectral emissions compared to those subcarriers located at the center of the band. Realizing this fact, the method in [56] proposes the use of heavy windowing on edge

subcarriers and light windowing on inner subcarriers. Heavy windowing is achieved by increasing the length of the window extensions applied to edge subcarriers. However, in order to maintain the spectral efficiency, those extra extensions are stolen from the CP duration of edge subcarriers. This can potentially create ISI as the CP of edge subcarriers is shortened. Nonetheless, this ISI can be avoided by proper scheduling of subcarriers in a multi-user environment [57].

2.5 Future Directions

Spectrum shaping is an important research problem that will continue to gain more attention, especially as we move towards cognitive radio based systems. Viable solutions are still needed as most of the algorithms proposed to date achieve sidelobe suppression at the expense of other performance metrics (BER, spectral efficiency, PAPR, complexity). No algorithm achieves the best trade-off among all performance factors. Additionally, the most promising techniques such as precoding, while they are capable of achieving deep sidelobe suppression and show flexibility in shaping the power spectrum through the choice of their notching frequencies, their implementation comes with a huge increase in the computational complexity that renders most them impractical for real time applications. This is true for other techniques as well, where most of them have computational complexity that grows with the number of subcarriers used. Given the ever increasing demand for high data rate transmission which requires the use of more subcarriers to satisfy such a demand. This means that most of the methods discussed in this review are not suitable for current and future broadband communications systems. In fact, the only method the offers tractable computational complexity is the time domain windowing method, however, its suppression performance does not satisfy the requirements of cognitive radio systems, especially in inner bands unless the spectral efficiency is significantly traded off. Therefore, there is a need for computationally tractable solutions that offer reasonable sidelobe suppression for the requirements of cognitive radio without trading off the spectral efficiency.

Recent trends have shown increased interest in FBMC as a replacement for OFDM as the signaling scheme of choice for the PHY layer of cognitive radios due to the low spectral sidelobes it offers [58, 59]. However, such a move entails huge changes to the current standards such as

LTE, WiMax, WiFi, etc, that adopted OFDM in their PHY layer. Moreover, FBMC suffers from the same complexity issues that OFDM combined with sidelobe suppression algorithms suffers from. Therefore, we believe that OFDM coupled with better low complexity sidelobe suppression algorithms is the better option moving forward.

2.6 Conclusions

OFDM has proven its worth in broadband communications and is therefore considered the signaling scheme of choice for cognitive radio applications due to the many advantages it offers including simple equalization, spectral efficiency and robustness against multipath fading channels. Despite these advantages, it suffers from high spectral sidelobes that create significant interference to users operating in adjacent channels. In this chapter, we presented a review of the most important sidelobe suppression algorithms and provided a framework under which most of these algorithms can be explained. We showed the impact of these techniques on the performance metrics of OFDM. Additionally, we highlighted the limitations of these algorithms and showed that current solutions for the spectrum shaping problem are not suitable for upcoming broadband wireless communications systems due to the prohibitive computational complexity that comes along with the implementation of these methods.

CHAPTER 3

MASK COMPLIANT PRECODER

3.1 Introduction

Most sidelobe suppression schemes focus on minimizing the out-of-band spectrum or forcing it to zero. In this chapter[1], we question such an approach and instead present a precoder that renders the power spectrum of OFDM signals below a given SEM. Ultimately, most standards only require the transmitted signal spectrum to fall under the RF mask. By following this approach, the distortion added to the information symbols in order to shape the spectrum will be kept at minimum levels. In essence, only a small adjustment of the information symbols is needed to force the spectrum below the mask. Our approach improves over the precoder proposed in [1] in that it maintains almost the same BER probability as uncoded OFDM without the need for any side information to be transmitted to the receiver.

The rest of the chapter is organized as follows. In Section 3.2, the system model is presented. We introduce the mask compliant precoder in Section 3.3 and the simulation results in Section 3.4. Finally, the conclusion is drawn in Section 3.5.

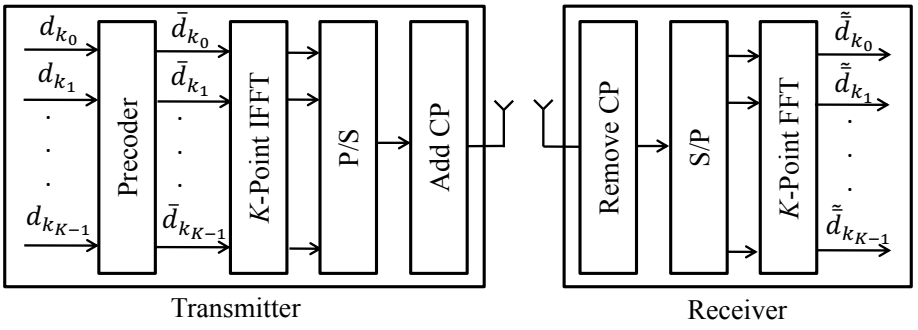

Figure 3.1 Block diagram of OFDM transmitter/receiver pair with sidelobe suppression.

[1]The contents of this chapter were published in [60]. Copyright permission is included in Appendix B.

3.2 System Model

Consider an OFDM system with $\mathcal{K} = \{k_0, k_1 ..., k_{K-1}\}$ subcarriers per symbol as shown in Figure 3.1. The QAM symbols $\mathbf{d} = [d_{k_0}, d_{k_1}, ..., d_{k_{K-1}}]^T$, where $(\cdot)^T$ is the transpose operation, are fed into the sidelobe suppression precoder to generate a new set of symbols $\bar{\mathbf{d}} = [\bar{d}_{k_0}, \bar{d}_{k_1}, ..., \bar{d}_{k_{K-1}}]^T$, chosen in such a way to provide better spectral emissions. The generated vector $\bar{\mathbf{d}}$ is then used to modulate the K subcarriers using the inverse fast Fourier transformation (IFFT). The resulting parallel data stream is transformed to a single stream with the parallel-to-serial (P/S) converter, and a CP of length greater than the maximum excess delay of the channel is added to combat the effect of ISI. The expression of the OFDM symbol can then be written as

$$s(t) = \sum_{k=0}^{K-1} \bar{d}_k e^{j2\pi \frac{k}{T_s} t} R_c(t) \ , \tag{3.1}$$

where $R_c(t)$ is a window function and T_s is the effective symbol time. In this work, we only consider an OFDM system with a rectangular window defined by

$$R_{\mathrm{c}}(t) = \begin{cases} 1 \ , & \frac{-T}{2} < t < \frac{T}{2} \\ 0 \ , & \text{otherwise} \end{cases} \ , \tag{3.2}$$

where $T = T_{\mathrm{s}} + T_{\mathrm{cp}}$ and T_{cp} is the cyclic prefix duration. At the receiver, the CP is removed and the data symbols are demodulated with the FFT to produce the received symbols $\tilde{\bar{\mathbf{d}}}$, which are mapped *directly* to the original symbols $\mathbf{d}$.

3.3 Mask Compliant Precoder

We will follow the same analysis in [1]. The Fourier transform of the OFDM symbol in (3.1) is given by

$$S(f) = \sum_{k=0}^{K-1} \bar{d}_k a_k(f) = \mathbf{a^T}(\mathbf{f})\bar{\mathbf{d}} \ , \tag{3.3}$$

where $a_k(f) = \int_{-\frac{T}{2}}^{\frac{T}{2}} e^{\frac{j2\pi k}{T_s}t} e^{-j2\pi ft} dt = \text{sinc}\left(T(f - \frac{k}{T_s})\right)$ and $\mathbf{a(f)} = [a_{k_0}(f), a_{k_1}(f), ..., a_{k_{K-1}}(f)]^T$. The resulting sinc functions are the main reason that OFDM signals exhibit high sidelobes in the out-of-band region. According to [1], the power spectrum of (3.1) is obtained as

$$P(f) = \frac{1}{T} E\{|S(f)|^2\} \ . \tag{3.4}$$

Instead of forcing the power spectrum to zero, our goal in this chapter is to keep the spectrum at a set of predefined frequencies in the out-of-band region below a given RF mask. We first sample the spectrum of the transmitted signal at M frequency locations $f_m \in \{f_0, f_1, ..., f_{\text{M}-1}\}$ in the out-of-band region. After collecting the M samples $[S(f_0), S(f_1), ..., S(f_{\text{M}-1})]^T$ in the vector $\mathbf{S}$, the out-of-band spectrum resulting from the precoded symbols $\bar{\mathbf{d}}$ can then be given from (3.3) by

$$\mathbf{S} = \mathbf{A}\bar{\mathbf{d}} \ , \tag{3.5}$$

where $\mathbf{A} = [\mathbf{a}(f_0), \mathbf{a}(f_1), ..., \mathbf{a}(f_{\text{K}-1})]^T$ is an $M \times K$ matrix with entries $a_k(f_m)$ representing the sidelobe interference from the kth subcarrier at the discrete frequency f_m in the out-of-band region.

Since our main objective is to control the spectrum emissions under a specified RF mask, we therefore require the power of every sample in $\mathbf{S}$, i.e., $|S(f_m)|^2$, to fall underneath the mask. Using (3.5), this is equivalent to

$$|[\mathbf{A}\bar{\mathbf{d}}]_i|^2 \leq [\mathbf{b}]_i \ . \tag{3.6}$$

where $\mathbf{b}$ is an $M \times 1$ vector containing the RF mask samples, $[\mathbf{A}\bar{\mathbf{d}}]_i$ and $[\mathbf{b}]_i$ represent the ith entry of vectors $\mathbf{A}\bar{\mathbf{d}}$ and $\mathbf{b}$, respectively.

There are many solutions $\bar{\mathbf{d}}$ that satisfy (3.6), but we are only interested in the vector $\bar{\mathbf{d}}$ that is closest to the original data vector $\mathbf{d}$ in terms of euclidean distance. That is, we require the precoded symbols to fall in the same decision region as the original data symbols. This is to ensure that the BER probability is not greatly affected by the precoding operation.

Our precoder is then the solution to

$$\min_{\bar{\mathbf{d}}} \|\mathbf{d}-\bar{\mathbf{d}}\|_{\mathbf{2}}^{\mathbf{2}} \;\text{ subject to }\; |[\mathbf{A}\bar{\mathbf{d}}]_i|^2 \leq [\mathbf{b}]_i \;. \tag{3.7}$$

In (3.7), $|[\mathbf{A}\bar{\mathbf{d}}]_i|^2 \leq [\mathbf{b}]_i$ imposes M inequality constraints that represent the power spectrum values at the M frequency locations in the out-of-band region, which can instead be written as

$$-\sqrt{[\mathbf{b}]_i} \leq [\mathbf{A}\bar{\mathbf{d}}]_i \leq \sqrt{[\mathbf{b}]_i} \;. \tag{3.8}$$

Alternatively, the M constraints in (3.8) can be represented in a more compact way as

$$\underbrace{\begin{bmatrix} \mathbf{A} \\ -\mathbf{A} \end{bmatrix}}_{\tilde{\mathbf{A}}} \bar{\mathbf{d}} \leq \underbrace{\begin{bmatrix} \sqrt{\mathbf{b}} \\ \sqrt{\mathbf{b}} \end{bmatrix}}_{\tilde{\mathbf{b}}} \;, \tag{3.9}$$

where $\sqrt{\mathbf{b}}$ is the element-wise square root of vector $\mathbf{b}$. Thus, (3.7) can be rewritten as

$$\min_{\bar{\mathbf{d}}} \|\mathbf{d}-\bar{\mathbf{d}}\|_{\mathbf{2}}^{\mathbf{2}} \;\text{ subject to }\; \tilde{\mathbf{A}}\bar{\mathbf{d}} \leq \tilde{\mathbf{b}} \;. \tag{3.10}$$

The objective function along with the constraints in (3.10) can be cast as a quadratic programming problem with linear inequality constraints. Its solution leads to a precoder that properly maps the information symbols $\mathbf{d}$ to a new set of symbols $\bar{\mathbf{d}}$, having spectral emissions *fully contained* under the RF mask $\mathbf{b}$, and more importantly, it ensures that the new symbols $\bar{\mathbf{d}}$ are close to $\mathbf{d}$ in the euclidean distance sense. Many efficient numerical algorithms exist that can solve such an optimization problem such as the interior-point-convex algorithm [61]. However and to the best of our knowledge, there is no closed-form solution for the precoder in (3.10), we herein use numerical methods to evaluate its performance.

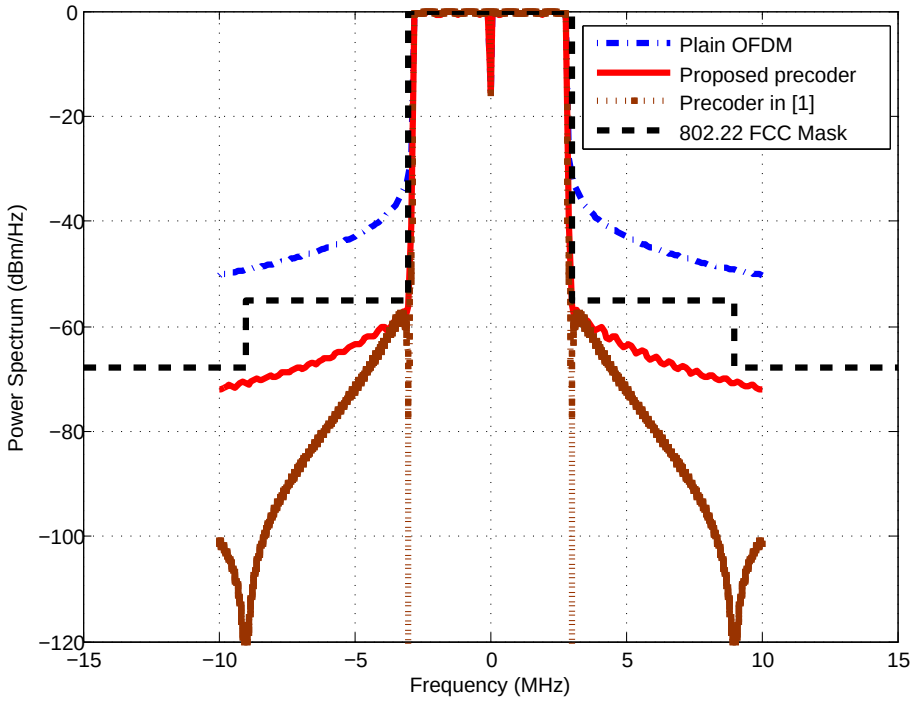

Figure 3.2 Power spectrum under a strict mask.

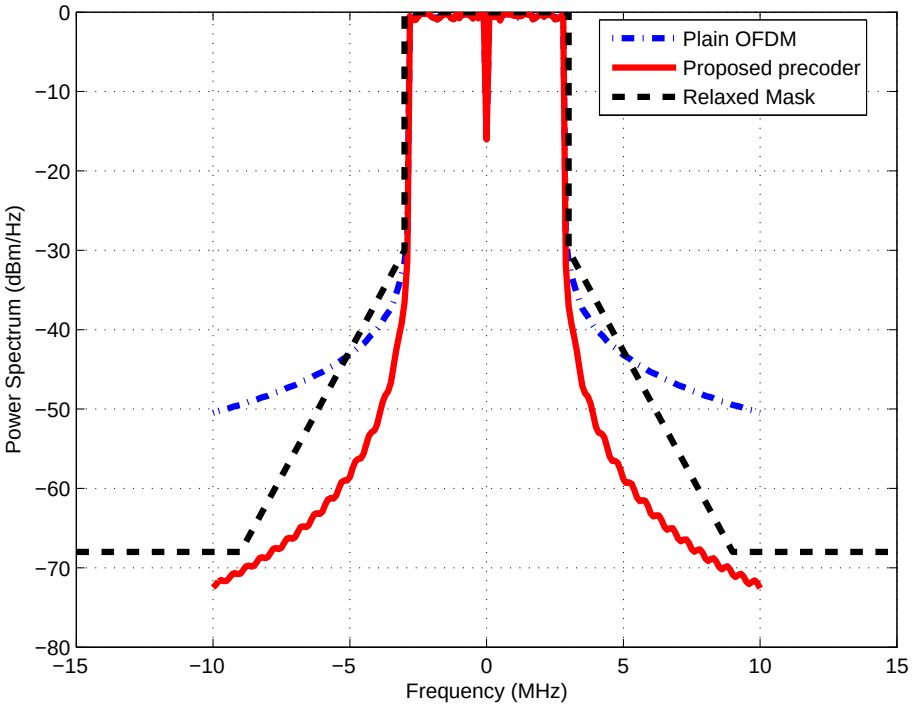

Figure 3.3 Power spectrum under a relaxed mask.

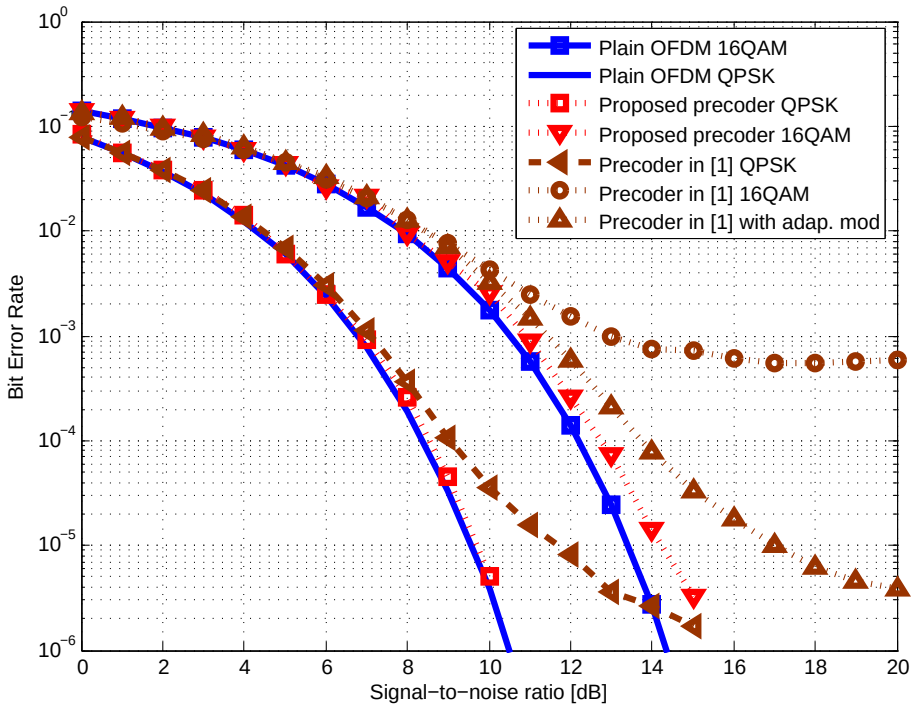

Figure 3.4 BER performance of the proposed precoder under a relaxed mask and the precoder [1] in AWGN channels, compared with conventional OFDM.

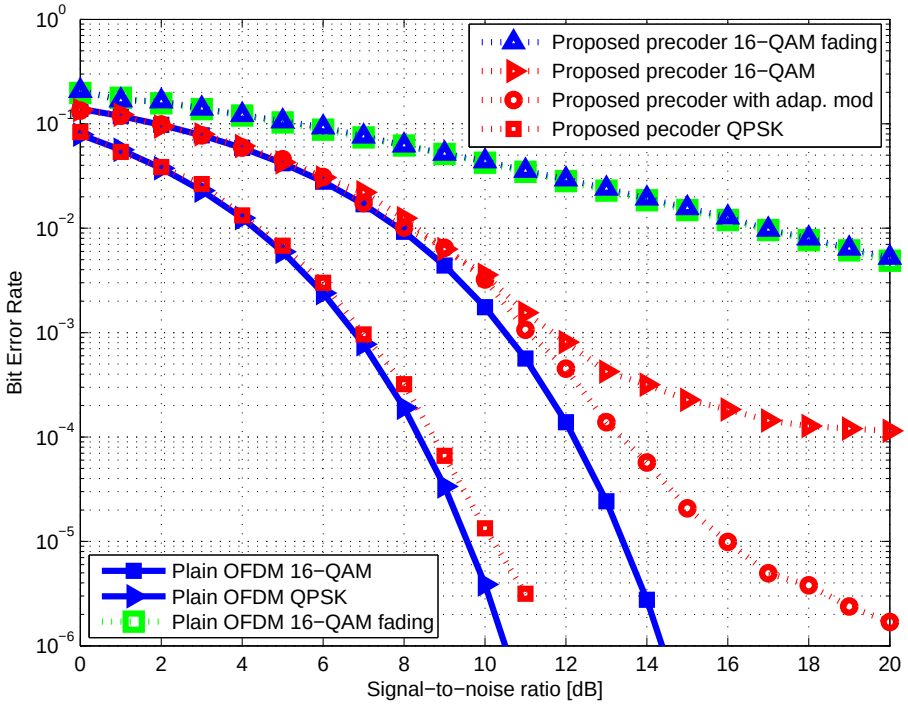

Figure 3.5 BER performance of the proposed precoder in AWGN and a multipath Rayleigh fading channels under a strict mask, compared with conventional OFDM.

Table 3.1 Simulation parameters for IEEE 802.22 WRAN.

Parameter	Value
Channel bandwidth	6 MHz
FFT size	2048
Number of used subcarriers (K)	1680
FFT window duration (T_{s})	$\frac{896}{3}$ μs
CP duration (T_{cp})	$\frac{28}{3}$ μs

3.4 Simulation Results

Performance of the proposed precoder is investigated using computer simulations. Our simulation parameters are based on the recent draft of the IEEE 802.22 WRAN standard and are summarized in Table 3.1. The number of frequency samples in the out-of-band region is set to only 5 samples[2] per 1 MHz of bandwidth. To control the sidelobes under the RF mask, we consider a bandwidth of 7 MHz on each side of the spectrum, resulting in $M = 70$ samples. We evaluated the performance of the precoder under both strict and relaxed masks. The power spectral density of OFDM signals with and without precoding along with the RF mask are provided in Figure 3.2 and Figure 3.3. While the precoder in [1] provides deeper suppression than our proposed precoder as shown Figure 3.2, this extra suppression is unnecessary and comes at the expense of a loss in BER performance, as will be discussed below. This is particularly important for the relaxed mask in Figure 3.3, where only a small distortion added to the information symbols is needed to force the out-of-band emissions below the mask.

Error probabilities of the proposed precoder and the precoder in [1] are shown in Figure 3.4 and Figure 3.5. Since the distortion added to the information symbols depends on the prescribed RF mask, the symbols are slightly distorted when the relaxed mask of Figure 3.3 is used, leading to BER curves similar to those of uncoded OFDM as reported in Figure 3.4. This is in contrast to the precoder in [1] which heavily distorts the information symbols regardless of the RF mask being used. Specifically, the proposed precoder improves over the precoder presented in [1] which has an

[2]Smaller number of samples are possible by choosing pairs of frequencies close to each other. Results in [1] show that selecting pairs of frequencies close to each other improves the spectral suppression. For example, the frequency set $\{\pm 3001 \pm 1, \pm 3901 \pm 1, \pm 6901 \pm 1, \pm 9001 \pm 1, \pm 9901 \pm 1\}$ kHz achieves the same results as in Figure 3.2 and Figure 3.3. However, with this choice of smaller samples the information symbols have to be distorted heavily in order to keep the spectrum under the mask leading to a slight degradation in BER.

error floor and its performance diverges from uncoded OFDM at around 6 dB SNR for both QPSK and 16-QAM. A better alternative to the precoder in [1] is the orthogonal multiplexing precoder presented in [29]. It forces the out-of-band spectrum to zero without causing any degradation in the BER performance. However, it does so by sacrificing some of the signal dimensions for the sake of spectral suppression and therefore reduction of the system throughput is unavoidable. By allowing a slight degradation in the BER, the proposed precoder can be an alternative to the one in [29] with no reduction in the data rate at all, particularly under relaxed masks.

Although the proposed precoder is capable of containing the spectral emissions under the more strict mask of Figure 3.2, its BER performance in AWGN channels for 16-QAM deteriorates compared to plain OFDM. However, it should be noted that the BER for QPSK follows that of uncoded OFDM for a good range of practical SNR values as shown in Figure 3.5. Furthermore, these BER curves are obtained with the assumption that the distribution of the distortion vector $\mathbf{w}$, where $\mathbf{w} = \mathbf{d} - \bar{\mathbf{d}}$, is Gaussian and the detector used is a minimum distance detector. Nonetheless, the BER performance can be further improved by considering an optimum detector based on the statistical properties of the noise vector $\mathbf{w}$. However, this is beyond the scope of this chapter and we therefore leave such analysis for future studies. In multipath Rayleigh fading channels, the distortion caused by the channel dominates the small distortion added by the proposed precoder leading to BER performance similar to that of conventional OFDM as shown in Figure 3.5.

An interesting result, though expected, is that both the precoder (3.10) and the one in [1] cause more distortion on edge subcarriers in order to suppress the sidelobes. This is particularly the case since edge subcarriers create more interference in the out-of-band region compared to inner subcarriers. Consequently, this leads to more errors on edge subcarriers as illustrated by the error vector magnitude (EVM) per subcarrier in Figure 3.6. Since edge subcarriers are heavily distorted by the precoding operation, the overall BER performance can be further improved by using adaptive modulation. The simulation results in Figure 3.4 and Figure 3.5 illustrate the remarkable improvement in the BER of both precoders when lower order modulation, i.e., QPSK instead of 16-QAM, is used on the edge subcarriers $k \in \{-840{:}-800\ 800{:}840\}$. The BER improves by two orders of magnitude from 10^{-4} to approximately 10^{-6} at 20 dB SNR. Certainly, more edge

subcarriers can be used to further improve the BER curves. However, the price will be paid by some reduction in the system throughput. Therefore, the proposed method when combined with adaptive modulation based on subcarrier EVM values, provides a trade-off between error performance and spectral efficiency. It's worth noting that adaptive modulation is not needed in the case of a relaxed mask as the BER curves are virtually the same as uncoded OFDM.

Unlike the precoders in [1] and [29], the proposed precoder needs to search for the proper symbols for each OFDM signal by solving the quadratic program in (3.10). This might lead to an increase in the computational complexity. However, algorithms such as the interior-point-convex method can solve quadratic programming problems such as the one in (3.10) in a polynomial time if the coefficient matrix of the objective function is positive definite. Fortunately, the coefficient matrix of the objective function in (3.10) is the identity matrix, which is positive definite, leading to significant reduction in the computational complexity. In addition, the computational complexity of the proposed precoder grows with the dimension of the matrix $\mathbf{A}$. However, since edge subcarriers contribute significantly to the out-of-band emissions, the complexity can be reduced by considering only the out-of-band contributions from edge subcarriers in the matrix $\mathbf{A}$. The price paid for this reduction will be some loss in BER performance, since edge subcarriers will be extremely distorted in order to the suppress the sidelobes, as opposed to when all subcarriers are used. Furthermore, instead of requiring the power spectrum to fall below the RF mask at individual frequency locations in the out-of-band region, a different metric such as ACLR can be used. By requiring the average power spectrum, i.e., ACLR to be below a given value, the computational complexity can be reduced significantly.

3.5 Conclusion

A precoder that forces the power spectrum of OFDM signals under a given RF mask is proposed. The proposed precoder provides significant improvement in BER performance compared to the precoder in [1], especially when operating under relaxed masks. Although the BER performance deteriorates under strict masks for 16-QAM, it remains virtually unaffected in the case of QPSK for a good range of practical SNR values. Moreover, with the use of adaptive modulation,

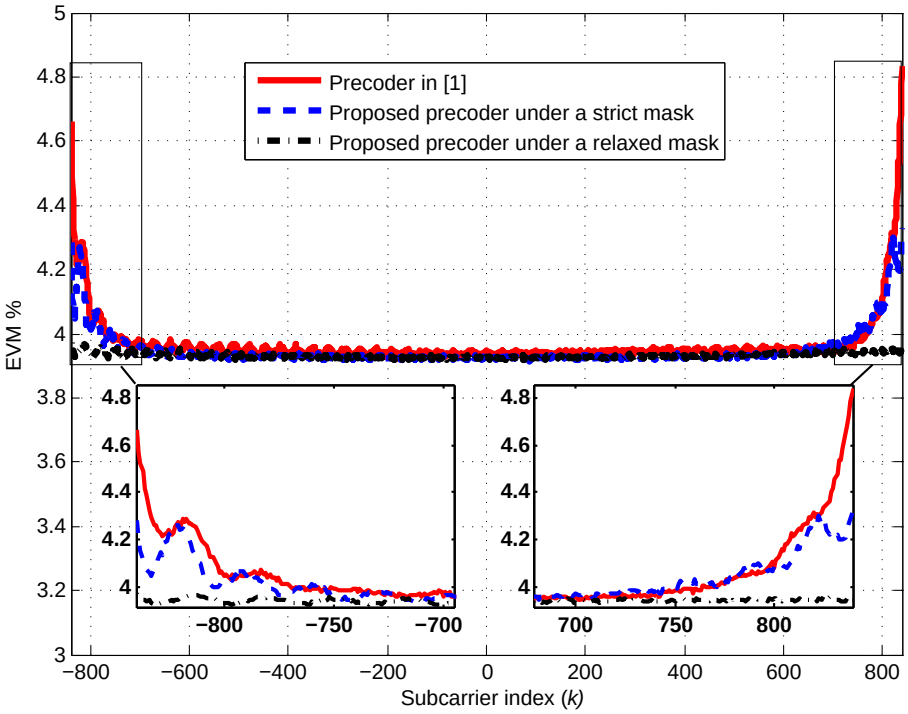

Figure 3.6 EVM per subcarrier for the proposed precoder and the precoder in [1] for QPSK.

the BER performance under strict masks can be further improved. Finally, the proposed precoder does not require the transmission of any side information to the receiver.

CHAPTER 4

SUPPRESSING ALIGNMENT: JOINT PAPR AND OUT-OF-BAND POWER LEAKAGE REDUCTION FOR OFDM-BASED SYSTEMS

4.1 Introduction

In this chapter, we target the joint reduction of both PAPR and OOB emissions of OFDM signals. Almost all existing solutions for the OOB leakage reduction suffer from either a spectral efficiency loss or BER degradation. Furthermore, most spectral suppression algorithms ignore the issue of high PAPR, an inherent characteristic of OFDM waveforms. As a result, the gains in OOB leakage reduction provided by these algorithms might be misleading, i.e., the spectral sidelobes can potentially grow back up after the high peak power transmitted signal passes through the PA. Therefore, and for the reasons outlined above, particularly the spectral regrowth problem, we believe that the best way is to address the two problems jointly as done in [44, 62–64]. Following this path, we herein propose a novel algorithm, that we call *suppressing alignment*, for the joint suppression of both the OOB leakage and PAPR without any reduction in the transmission rate. Our algorithm exploits the temporal degrees of freedom provided by the CP, a necessary redundancy in OFDM systems, to properly design a suppressing signal that can effectively reduce both the OOB power leakage and PAPR of the OFDM signal. In particular, our approach adds another dimension to the use of the CP. Traditionally, the CP has been exploited mainly to mitigate the impact of ISI in multipath fading channels. In this work, we extend that functionality by also utilizing the CP for the purpose of spectral emissions suppression and PAPR reduction. Besides exploiting the CP, our design also utilizes the wireless channel to align the generated suppressing signal with the CP duration of the OFDM symbol at the receiver. By doing so, the suppressing signal will not cause any interference to the data portion of the OFDM symbol. From an interference point of view, the data carried in the OFDM symbol appears to be corrupted by the suppressing signal at the

transmitter. However, after passing through the channel, the suppressing signal is perfectly aligned with the CP. In light of such alignment, the data portion of the OFDM symbol appears completely free of interference to the receiver. Thus, after discarding both the CP and the aligned suppressing signal through a simple CP removal operation, the receiver can decode the data with an error performance similar to that of standard OFDM. In addition to maintaining a spectral efficiency and error performance similar to plain OFDM, another advantage of our approach is that it does not require any change in the receiver structure of legacy OFDM.

Similar approaches, albeit for different purposes, have previously been proposed in [65] for interference alignment in two-tierd networks, in [66] for improving the secrecy rate of OFDM systems, and very recently in [67] for energy harvesting. Nevertheless, we believe that this is the first approach that exploits such a design for the purpose of spectral emissions and PAPR containment.

The rest of the chapter is organized as follows. In Section 4.2, the system model is introduced. The concept of suppressing alignment and its application to the reduction of OOB leakage is presented in Section 4.3. The joint reduction of OOB leakage and PAPR is presented in Section 4.4. In Section 4.5, we provide the numerical results and finally the conclusion is provided in Section 4.6.

In this chapter, $\mathbf{I}_N$ is the $N \times N$ identity matrix; $\mathbf{0}_{N\times M}$ is an all zeros $N \times M$ matrix. The transpose and conjugate transpose are denoted by $(\cdot)^{\mathrm{T}}$ and $(\cdot)^{\mathrm{H}}$, respectively, and $\|\cdot\|_2$ denotes the 2-norm. $\mathbb{E}[\cdot]$ denotes the expectation operator while $\ker(\cdot)$ denotes the kernel of the matrix. The field of real and field of complex numbers are represented by $\mathbb{R}$ and $\mathbb{C}$, respectively. $\mathcal{CN}(\mu, \Sigma)$ is the complex Gaussian distribution with mean μ and covariance matrix Σ.

4.2 System Model

We consider a single link OFDM system consisting of a transmitter and a receiver communicating over a Rayleigh multipath channel as shown in Figure 4.1. For ease analysis and without any loss of generality, we assume an adjacent user, employing OFDM or any other technology, operating over a bandwith spanning K subcarriers within the transmission band of the OFDM system. Therefore, the OFDM transmitter/receiver pair should control their transmissions such

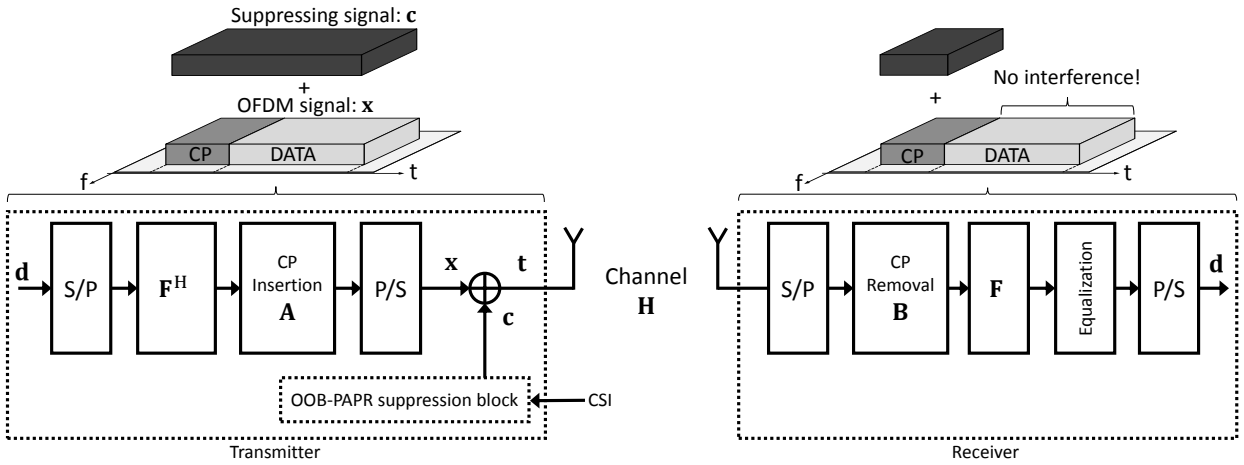

Figure 4.1 System model of an OFDM transmitter and receiver with suppressing alignment.

that minimal interference is caused to this adjacent user. Let the total number of subcarriers be N, where the subcarriers spanning the adjacent user band, i.e., $\{i+1, ..., i+K\}$, are deactivated. The remaining active subcarriers $\{1, ..., i\} \cup \{i+K+1, ..., N-1\}$, whereas the DC subcarrier is disabled, are modulated by the set of QAM symbols contained in the vector $\mathbf{d} \in \mathbb{C}^{N\times 1}$. To mitigate the effects of ISI, a CP of length L samples, which is assumed to be larger than the maximum delay spread of the channel, is added to the start of the OFDM symbol. The resulting time domain OFDM signal is expressed in vectorized form as

$$\mathbf{x} = [x_1, ..., x_{N+L}]^{\mathrm{T}} = \mathbf{A}\mathbf{F}^{\mathrm{H}}\mathbf{d} \ , \tag{4.1}$$

where $\mathbf{F}$ is the N-point discrete Fourier transformation (DFT) matrix, and $\mathbf{A} \in \mathbb{R}^{(N+L)\times N}$ is the CP insertion matrix defined as

$$\mathbf{A} = \begin{bmatrix} \mathbf{0}_{L\times N-L} & \mathbf{I}_L \\ & \mathbf{I}_N \end{bmatrix} \ .$$

To control the spectral emissions of the transmitted signal as well as its PAPR, the OOB-PAPR suppression block generates a time-domain *suppressing signal* $\mathbf{c} = [c_1, ..., c_{N+L}]^{\mathrm{T}}$ with the same length as the OFDM signal, i.e., $\mathbf{c} \in \mathbb{C}^{(N+L)\times 1}$. Furthermore, let the suppressing signal $\mathbf{c}$ be

expressed as

$$\mathbf{c} = \mathbf{P}\mathbf{s} \ , \tag{4.2}$$

where $\mathbf{P} \in \mathbb{C}^{(N+L)\times L}$ and $\mathbf{s} \in \mathbb{C}^{L\times 1}$. The transmitted signal is then given as

$$\mathbf{t} = \mathbf{x} + \mathbf{c} = \mathbf{A}\mathbf{F}^{\mathrm{H}}\mathbf{d} + \mathbf{P}\mathbf{s} \ . \tag{4.3}$$

The design of both $\mathbf{s}$ and $\mathbf{P}$ will be discussed in detail in the following section; however for the time being, it suffices to say that $\mathbf{c} = \mathbf{P}\mathbf{s}$ will be designed to suppress both the spectral sidelobes and PAPR of the transmitted signal.

4.3 Suppressing Alignment

In this section, we introduce the concept of suppressing alignment and discuss its use in suppressing the spectral emissions of the transmitted OFDM signal. The application of suppressing alignment in reducing the PAPR will be discussed in the next section. Our main aim in this section is to construct the suppressing signal $\mathbf{c}$ in (4.3) so that the transmitted signal has better spectral emissions compared to conventional OFDM signals. More specifically, the suppressing signal $\mathbf{c}$ or equivalently ($\mathbf{P}\mathbf{s}$) is designed under two goals in mind: 1) to minimize the OOB power leakage of the transmitted signal in the adjacent band and 2) to avoid causing any interference to the information data carried by the OFDM symbol, in the sense that the receiver is able to recover all information data sent by the transmitter. In the subsequent discussion, the vector $\mathbf{s}$ will be designed to fulfill the first requirement while the matrix $\mathbf{P}$ is designed to satisfy the latter.

We first consider the construction of the matrix $\mathbf{P}$. Since the suppressing signal is added to the OFDM signal before transmission in (4.3), the information data carried by the OFDM signal is distorted and the receiver might not be able to recover the data if the suppressing signal is not properly designed. To achieve such proper design, we need to examine the received signal at the receiver after passing through the channel.

Let the channel between the transmitter and receiver be an i.i.d. Rayleigh fading channel represented by the vector $\mathbf{h} = [h_0, ..., h_l] \sim \mathcal{CN}(0, \mathbf{I}_{l+1}/(l+1))$. We can then express the received signal as

$$\mathbf{r} = \mathbf{Ht} + \mathbf{n} \ , \tag{4.4}$$

where $\mathbf{H} \in \mathbb{C}^{(N+L)(N+L)}$ is a Toeplitz matrix used to model the convolution between the transmitted signal $\mathbf{t}$ and the channel $\mathbf{h}$ and is given by

$$\mathbf{H} = \begin{bmatrix} h_0 & 0 & \cdots & 0 & h_l & \cdots & h_1 \\ \vdots & \ddots & \ddots & \ddots & \ddots & \ddots & \vdots \\ \vdots & \ddots & \ddots & \ddots & \ddots & \ddots & h_l \\ h_l & \cdots & \cdots & h_0 & 0 & \cdots & 0 \\ 0 & \ddots & \ddots & \ddots & \ddots & \ddots & \vdots \\ 0 & \ddots & 0 & h_l & \cdots & \cdots & h_0 \end{bmatrix} \ ,$$

and $\mathbf{n} \in \mathbb{C}^{(N+L)\times 1} \sim \mathcal{CN}(0, \sigma^2 \mathbf{I}_{N+L})$ is an additive white Gaussian noise (AWGN) vector. Assuming perfect synchronization and after the serial-to-parallel (S/P) conversion, the receiver removes the first L CP samples and then applies DFT. Using (4.3), the received signal after CP removal and DFT operation can be written as

$$\mathbf{y} = \mathbf{FBHt} + \bar{\mathbf{n}} = \mathbf{FBHAF}^{\mathrm{H}}\mathbf{d} + \mathbf{FBHPs} + \bar{\mathbf{n}} \ , \tag{4.5}$$

where $\mathbf{B} \in \mathbb{R}^{N\times(N+L)}$ is the CP removal matrix and $\bar{\mathbf{n}} \in \mathbb{C}^{N\times 1}$ is a noise vector obtained after removing the first L samples from $\mathbf{n}$ and applying the DFT.

We are now ready to address the design of the matrix $\mathbf{P}$ by examining (4.5). As stated before, our goal in designing $\mathbf{P}$ is that the interference caused by the added suppressing signal

should be zero at the receiver. Therefore, the following must hold true

$$\mathbf{FBHPs} = \mathbf{0} \ . \tag{4.6}$$

If (4.6) is satisfied, then, the received vector $\mathbf{y}$ in (4.5) becomes similar to legacy OFDM received data and the receiver would be able to apply single-tap equalization to recover the information symbols. Essentially, the information data in the vector $\mathbf{d}$ experiences zero interference from the suppressing signal.

Assuming perfect channel state information (CSI) at the transmitter, it is clear from (4.6) that if $\mathbf{P}$ belongs to the null-space of the matrix $\mathbf{BH}$, i.e., $\ker(\mathbf{BH})$, then (4.6) is satisfied regardless of the value of the vector $\mathbf{s}$. Using the rank-nullity theorem, the dimension of the null-space of $\mathbf{BH} \in \mathbb{C}^{N\times(N+L)}$ is obtained as $\dim(\ker(\mathbf{BH})) = N + L - \text{rank}((\mathbf{BH})) = L$, since $\text{rank}(\mathbf{BH}) = N$. Hence, by choosing $\mathbf{P}$ such that its columns span $\ker(\mathbf{BH})$, the condition in (4.6) is satisfied and the receiver can recover the data using legacy OFDM reception. Accordingly, we design $\mathbf{P}$ such that

$$\text{span}(\mathbf{P}) = \ker(\mathbf{BH}) \ , \tag{4.7}$$

which is accomplished by choosing the columns of $\mathbf{P}$ as an orthogonal basis of $\ker(\mathbf{BH})$. Using the singular value decomposition, $\mathbf{BH}$ can be factorized as

$$\mathbf{BH} = \mathbf{U}\mathbf{\Sigma}\mathbf{V}^{\text{H}} \ , \tag{4.8}$$

where $\mathbf{U} \in \mathbb{C}^{N\times N}$, $\mathbf{\Sigma} \in \mathbb{C}^{N\times(N+L)}$ is a diagonal matrix holding the singular values of $\mathbf{BH}$, and $\mathbf{V} \in \mathbb{C}^{(N+L)\times(N+L)}$. If $\mathbf{V}$ is expressed as

$$\mathbf{V} = [\mathbf{v}_0 \ \mathbf{v}_1 \ ... \ \mathbf{v}_{N+L-1}] \ ,$$

then the last L columns of $\mathbf{V}$ constitute an orthogonal basis that spans the null-space of ($\mathbf{BH}$). Therefore, $\mathbf{P}$ is chosen as

$$\mathbf{P} = [\mathbf{v}_N \ \mathbf{v}_{N+1} \ ... \ \mathbf{v}_{N+L-1}] \ . \tag{4.9}$$

We remark that such construction of $\mathbf{P}$ allows interference-free transmission and is in principle similar to interference alignment (IA) [68]. In particular, $\mathbf{P}$ aligns the interference from the suppressing signal to the portion of the OFDM symbol spanned by the CP as shown in Figure 4.1.

We now consider the design of the vector $\mathbf{s}$. Before we go into the details of our proposed method, let's first examine the interference caused by the transmitted signal (4.3) over the K subcarriers occupied by the user in the adjacent band. The signal spectrum of the transmitted signal (4.3) is given as

$$\boldsymbol{\mathcal{S}}_t = \mathbf{F}_{\zeta N,\beta}(\mathbf{A}\mathbf{F}^{\mathrm{H}}\mathbf{d} + \mathbf{P}\mathbf{s}) \ , \tag{4.10}$$

where ζ is the upsampling factor, i.e., ζ samples per subcarrier are considered, $\beta = N + L$, and $\mathbf{F}_{\zeta N,\beta}$ is an $\zeta N \times \beta$ DFT matrix. Using (4.10), the interference in the adjacent band can be given as

$$\boldsymbol{\mathcal{I}}_K = \boldsymbol{\mathcal{F}}_K(\mathbf{A}\mathbf{F}^{\mathrm{H}}\mathbf{d} + \mathbf{P}\mathbf{s}) = \underbrace{\boldsymbol{\mathcal{F}}_K\mathbf{A}\mathbf{F}^{\mathrm{H}}\mathbf{d}}_{\boldsymbol{\mathcal{F}}_\mathbf{d}} + \underbrace{\boldsymbol{\mathcal{F}}_K\mathbf{P}}_{\boldsymbol{\mathcal{F}}_\mathbf{s}}\mathbf{s} \ , \tag{4.11}$$

where $\boldsymbol{\mathcal{F}}_K$ is a sub-matrix of $\mathbf{F}_{\zeta N,\beta}$ containing only the rows that correspond to the subcarriers occupied by the adjacent user. The first term in (4.11) represents the OOB power leakage from the information data and the second term is the OOB power leakage from the suppressing signal $\mathbf{c}$. To minimize the interference power in the adjacent band, we calculate $\mathbf{s}$ such that

$$\mathbf{s} = \arg\min_{\mathbf{s}} \|\boldsymbol{\mathcal{F}}_\mathbf{d} + \boldsymbol{\mathcal{F}}_\mathbf{s}\mathbf{s}\|_2 \ \text{ subject to } \ \|\mathbf{s}\|_2^2 \leq \epsilon \ , \tag{4.12}$$

where ϵ is a power constraint on the vector $\mathbf{s}$ to avoid spending too much power on the suppressing signal. We note here that the power of the suppressing signal $\mathbf{c}$ is equal to the power of the vector $\mathbf{s}$ since $\mathbf{P}$ is an orthogonal matrix. The optimization problem in (4.12) is known as a least squares with a quadratic inequality (LSQI) problem. To solve this problem, we first consider the unconstrained least squares problem, i.e., without the power constraint. The solution to the least squares problem is

$$\mathbf{s} = -(\boldsymbol{\mathcal{F}}_{\mathbf{s}}{}^{\mathrm{H}}\boldsymbol{\mathcal{F}}_{\mathbf{s}})^{-1}\boldsymbol{\mathcal{F}}_{\boldsymbol{s}}{}^{\mathrm{H}}\boldsymbol{\mathcal{F}}_{\mathbf{d}} \ . \tag{4.13}$$

It is clear that the calculated $\mathbf{s}$ in (4.13) is also the solution to the problem in (4.12) if $\|\mathbf{s}\|_2^2 \leq \epsilon$, and in this case we have an analytical solution. However, if $\|\mathbf{s}\|_2^2 \geq \epsilon$, then there is no analytical solution and in order to solve the problem, we have to consider the following unconstrained problem

$$\mathbf{s} = \arg\min_{\mathbf{s}} \|\boldsymbol{\mathcal{F}}_{\mathbf{d}} + \boldsymbol{\mathcal{F}}_{\mathbf{s}}\mathbf{s}\|_2 + \lambda_0\|\mathbf{s}\|_2^2 \ , \tag{4.14}$$

where $\lambda_0 > 0$ is the Lagrange multiplier. The solution in this case is

$$\mathbf{s} = -(\boldsymbol{\mathcal{F}}_{\mathbf{s}}{}^{\mathrm{H}}\boldsymbol{\mathcal{F}}_{\mathbf{s}} + \lambda_0\mathbf{I})^{-1}\boldsymbol{\mathcal{F}}_{\mathbf{s}}{}^{\mathrm{H}}\boldsymbol{\mathcal{F}}_{\mathbf{d}} \ . \tag{4.15}$$

For a proper Lagrange multiplier, which can be found using the bi-section search algorithm [69], $\|\mathbf{s}\|_2^2 = \epsilon$. Alternatively, (4.12) can be solved numerically using any of the publicly available optimization solvers.

4.4 Joint PAPR and OOB Power Leakage Reduction

PAPR is an important metric for multi-carrier systems. Any increase in the PAPR might drive the power amplifier at the transmitter to operate in the non-linear region. This can potentially cause spectral regrowth in the sidelobes, erasing any OOB reduction gains achieved before the power amplifier. Therefore, as an extension to the results in the previous section, we propose to jointly minimize the PAPR and OOB power leakage to avoid such problem.

The PAPR of the transmitted signal is the ratio of the maximum instantaneous power to the average power which is given as

$$\text{PAPR} = \frac{\|\mathbf{t}\|_\infty^2}{\frac{1}{(N+L)}\|\mathbf{t}\|_2^2} = \frac{\|\mathbf{x}+\mathbf{Ps}\|_\infty^2}{\frac{1}{(N+L)}\|\mathbf{x}+\mathbf{Ps}\|_2^2} \ . \tag{4.16}$$

Accordingly, to minimize the OOB interference as well as the PAPR, we extend the optimization problem in (4.12) as follows

$$\begin{aligned} &\mathbf{s} = \arg\min_{\mathbf{s}} (1-\lambda)\|\boldsymbol{\mathcal{F}}_\mathbf{d} + \boldsymbol{\mathcal{F}}_\mathbf{s}\mathbf{s}\|_2 + \lambda\|\mathbf{x}+\mathbf{Ps}\|_\infty \ , \\ &\text{subject to} \quad \|\mathbf{s}\|_2^2 \leq \epsilon \ , \end{aligned} \tag{4.17}$$

where the weighting factor, $\lambda \in [0,1]$, is for controlling the amount of minimization for both OOB power leakage and PAPR. This adaptation parameter can be flexibly adjusted to emphasize one problem over the other depending on the system design requirements. For example, when $\lambda = 0$, the objective function turns into a pure OOB power leakage reduction problem and (4.17) is equivalent to (4.12). On the other hand, (4.17) is a pure PAPR reduction problem when $\lambda = 1$. Similar to (4.12), the amount of power consumed by the suppressing signal is controlled by ϵ.

Both the objective function and the constraint in (4.17) are convex which renders the problem as a convex optimization problem that can easily be solved numerically by any convex optimization solver. In this work, we utilize YALMIP [70], a free optimization package that is easily integrated with MATLAB, and MOSEK [71] as the underlying solver to obtain a numerical solution to (4.17).

4.5 Numerical Results

In this section, we evaluate the OOB reduction as well as the PAPR performance of the proposed method with computer simulations. For simulation tractability, we consider an OFDM system with $N = 64$ subcarriers and a CP length of $L = 16$ samples. Additionally, we assume that the OFDM transmitter detects an adjacent user spanning 10 subcarriers within its band of transmission. Thus, these subcarriers are disabled by the OFDM system, while the remaining sub-

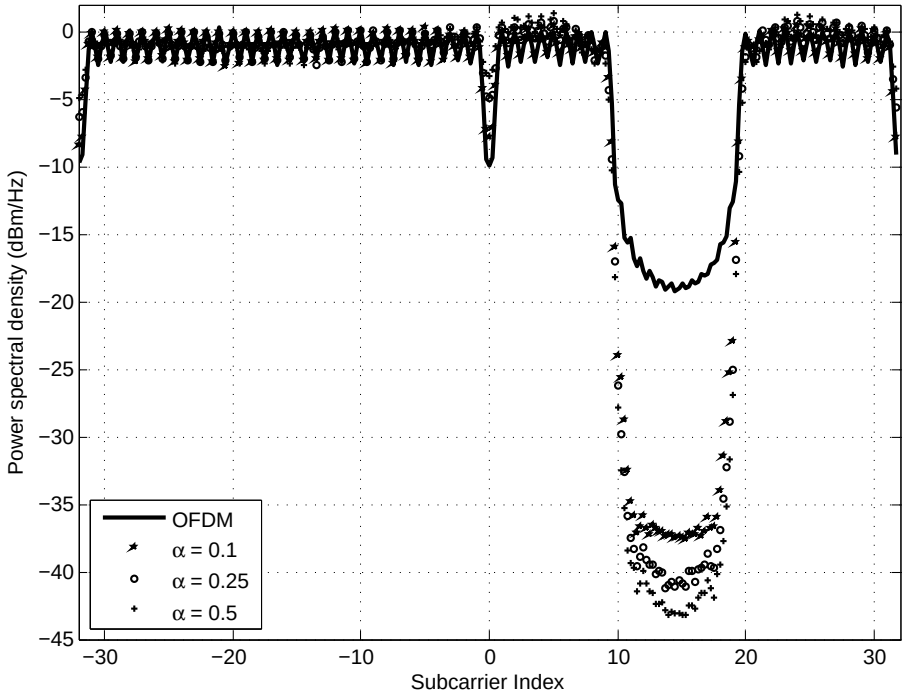

Figure 4.2 Power spectral density for 4-QAM.

carriers are utilized for transmission. The transmission is carried through a multipath Rayleigh fading channel with $L+1$ taps and a uniform power delay profile (PDP). To illustrate the OOB power leakage reduction performance of the proposed method, 10^4 M-QAM symbols are generated randomly, where $M = 4$ for QPSK or $M = 16$ for 16-QAM, and the Welch's averaged periodogram method is then used to estimate the power spectrum. We evaluate the the PAPR reduction performance using the complimentary cumulative distribution function (CCDF). Furthermore, in all simulations, we constrain the power of the suppressing signal to be a fraction of the power of the plain OFDM signal, i.e., $\epsilon = \alpha\|\mathbf{x}\|_2^2$, where α is a parameter that controls the power allocated to the suppressing signal.

4.5.1 PAPR and OOB Power Leakage Reduction Performance

First, we evaluate the OOB power leakage reduction of the proposed method based on (4.12), without considering the PAPR reduction. As shown in Figure 4.2, the proposed method achieves remarkable levels of OOB power leakage reduction compared to plain OFDM. We also

note that the amount of OOB power leakage reduction increases as α increases, i.e., as more power is allocated to the suppressing signal. For example, a 10% power increase in the transmitted signal power ($\alpha = 0.1$) reduces the OOB leakage by roughly 18 dB, while approximately 22 dB reduction is obtained for a 25% power increase. By examining Figure 4.2, we observe a slight overshoot in the spectrum close to the band edges, especially as α grows. This can be attributed to the fact that the suppressing signal puts more power on the subcarriers close to the edges because of their high contribution to the OOB power leakage.

Figure 4.3 shows the trade-off between the PAPR reduction and OOB reduction performance for the joint optimization problem in (4.17). The trade-off is visualized by showing the average reduction in both OOB leakage and PAPR as a function of the adaptation parameter λ when α is set to 0.25. We note that when $\lambda = 0$, the optimization problem (4.17) is equivalent to (4.12), where only the OOB interference is minimized. The average reduction in OOB interference in this case is approximately 22 dB, which agrees with the results in Figure 4.2 when $\alpha = 0.25$. Increasing λ beyond zero, reduces the gain in terms of OOB leakage reduction while gradually improving the PAPR reduction performance. As shown in Figure 4.3, a maximum average PAPR reduction of more than 3 dB is obtained when $\lambda = 1$. However, in this case, and as expected, there is no gain in the OOB interference reduction. In fact, the OOB power leakage increases due to the fact that the suppressing signal places some power in the adjacent band. The same is true when $\lambda = 0$, where a pure OOB leakage reduction leads to a slight increase in the PAPR as shown in Figure 4.3. The OOB power leakage reduction for different values of λ is shown in Figure 4.4. Here, the power of the suppressing signal is fixed at 25% of the original OFDM signal, i.e., $\alpha = 0.25$. These results in Figure 4.4 expand over the mean OOB reduction results in Figure 4.3 by showing the actual power spectral density of the transmitted signal. As seen from Figure 4.4, the OOB leakage is significantly reduced as λ decreases, which is rather expected as more emphasis is put on the OOB leakage reduction relative to the PAPR reduction. In order to understand the behavior of the joint optimization problem in (4.17) with regard to the actual power allocated to the suppressing signal, we plot the average power of the suppressing signal against α for different values of the adaptation parameter λ, as shown in Figure 4.5. The results in Figure 4.5 indicate that when

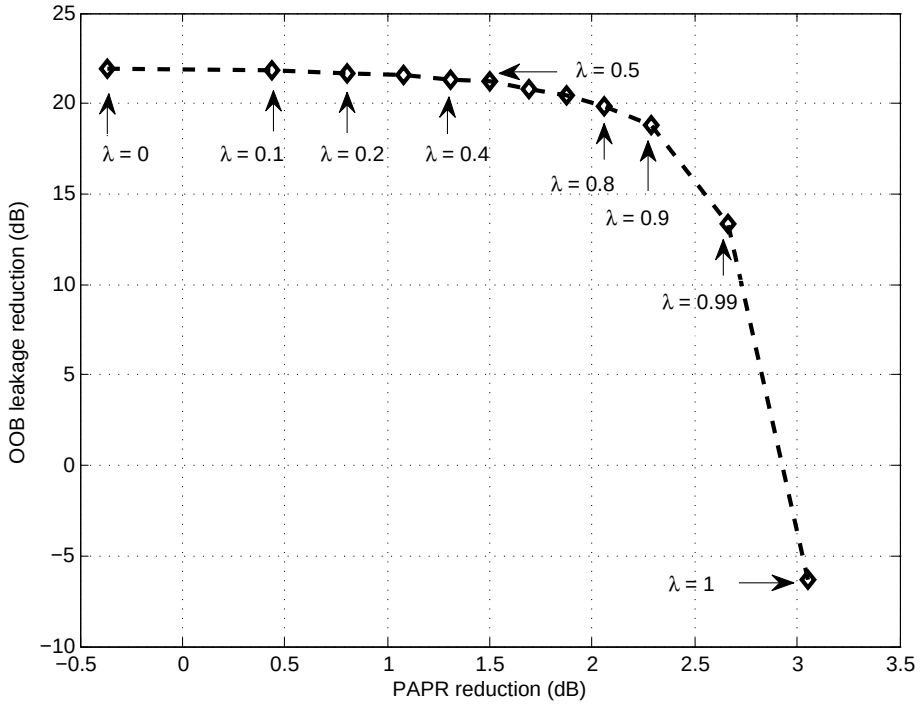

Figure 4.3 Performance trade-off between OOB reduction and PAPR reduction when $\alpha = 0.25$.

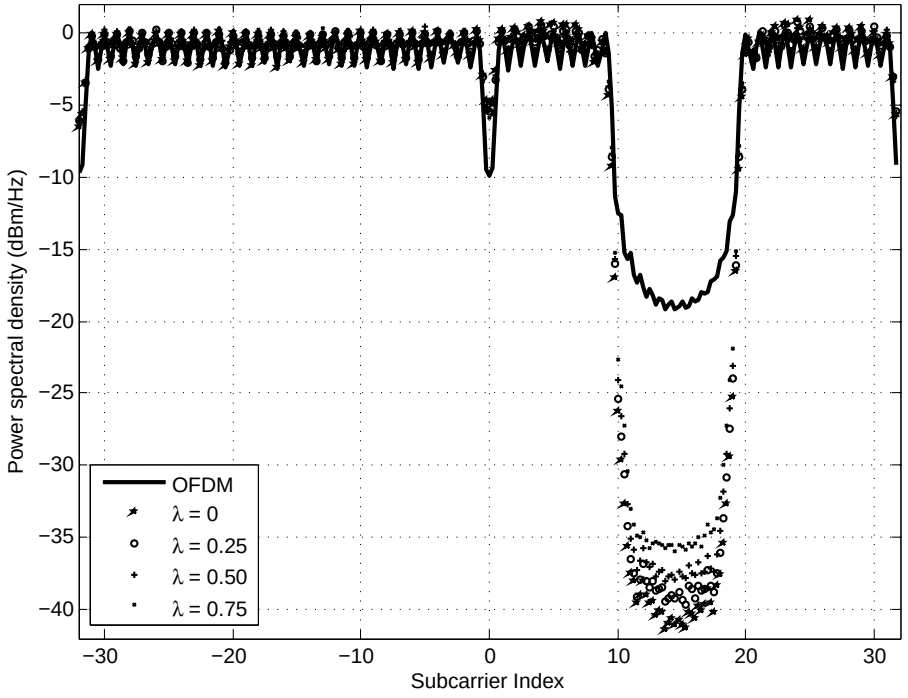

Figure 4.4 Power spectral density for 4-QAM for $\alpha = 0.25$.

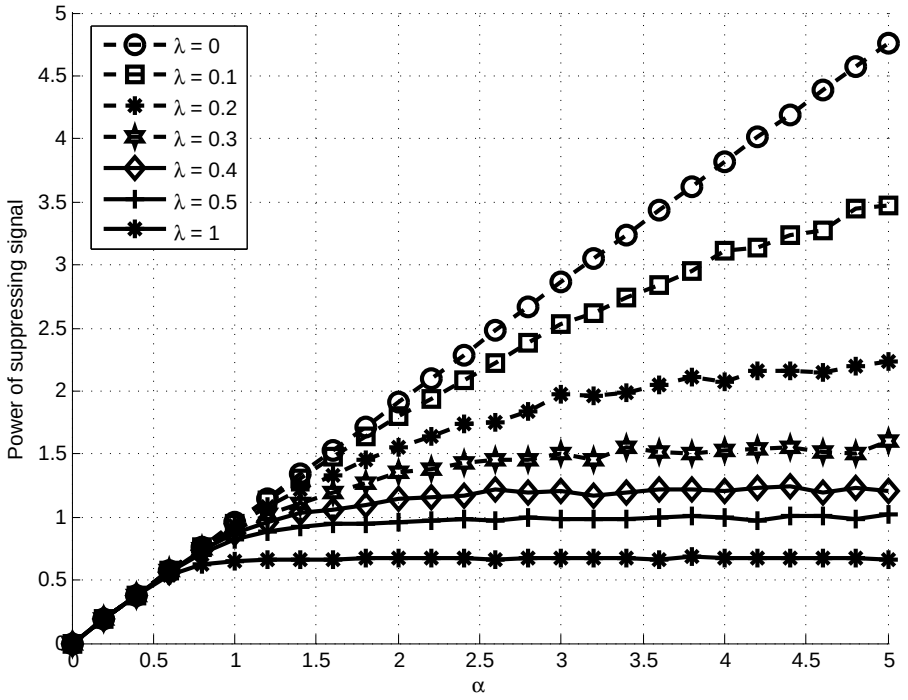

Figure 4.5 Power of suppressing signal for different values of λ.

the PAPR is not considered, i.e., $\lambda = 0$, the actual power used by the suppressing signal changes linearly with α. In other words, all power allocated to the suppressing signal will be completely utilized to reduce the spectral sidelobes. However, as the PAPR reduction is slowly factored into the problem, the utilization of the allocated power decreases. Specifically, we observe that as the adaptation parameter λ increases gradually, the suppressing signal uses less power to jointly reduce both PAPR and spectral leakage. For the extreme case of $\lambda = 1$, i.e., when it is a pure PAPR reduction problem, the power of the suppressing signal completely saturates regardless of how much power is allocated through the parameter α.

We now turn to characterizing the performance of the proposed method with regard to PAPR reduction. In order to do that, we consider the actual instantaneous power distribution of the transmitted signal and plot its CCDF as shown in Figure 4.6 and Figure 4.7. In Figure 4.6, we show the PAPR performance for different values of λ and a fixed $\alpha = 0.25$. We start by noting that remarkable reduction in the PAPR is obtained as shown in Figure 4.6. In particular, this reduction increases as the adaptation parameter λ grows, i.e., the PAPR reduction is emphasized

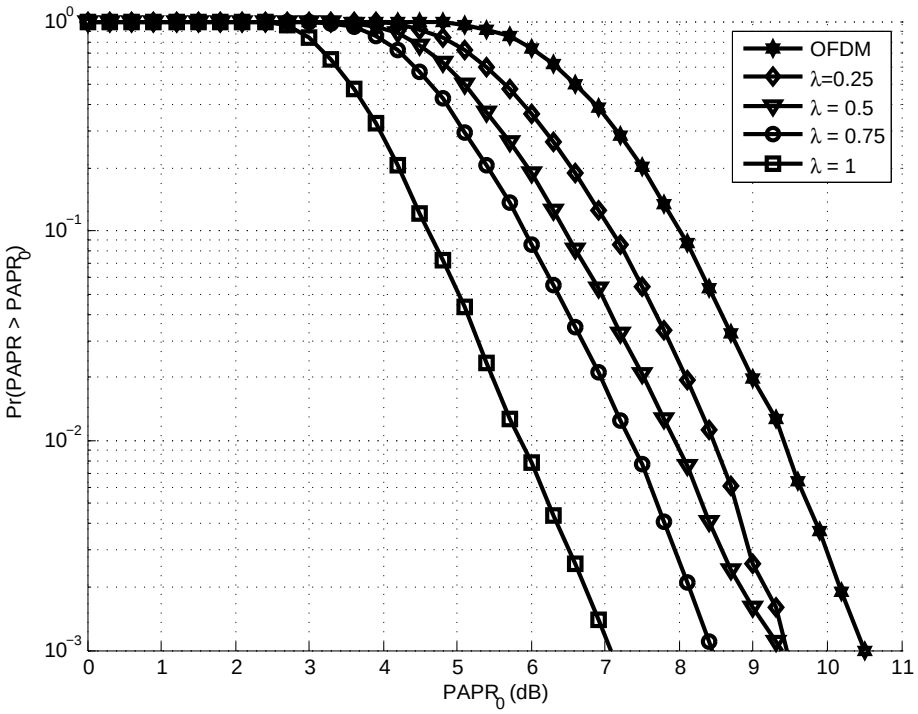

Figure 4.6 PAPR performance for 4-QAM when $\alpha = 0.25$.

compared to the power leakage reduction. For example, in the extreme case of $\lambda = 1$, the PAPR of the transmitted signal is around 7 dB at a probability of 10^{-3}; a reduction of approximately 3.5 dB from that of the plain OFDM signal. However, there is no reduction in the OOB interference when $\lambda = 1$. Nonetheless, decent improvements in the PAPR performance can still be obtained even for small values of λ while simultaneously allowing large reductions in the OOB interference. For example, when λ is set to 0.25, the PAPR of the transmitted signal is around 9.5 dB compared to 10.5 dB for plain OFDM. At the same value of λ, the OOB power of the transmitted signal is around -39 dB compared to -19 dB for plain OFDM; a 20 dB reduction as shown in Figure 4.4. The variation of the PAPR performance with the power of suppressing signal is shown in Figure 4.7. In the extreme case of having a suppressing signal with the same power as the OFDM signal, i.e., when $\alpha = 1$, the PAPR is reduced by approximately 4 dB at a probability of 10^{-3}. Alternatively, for $\alpha = 0.25$, the PAPR is reduced by approximately 1.5 dB, showing that a slight increase in the power of the transmitted signal can still lead to good reduction in the PAPR.

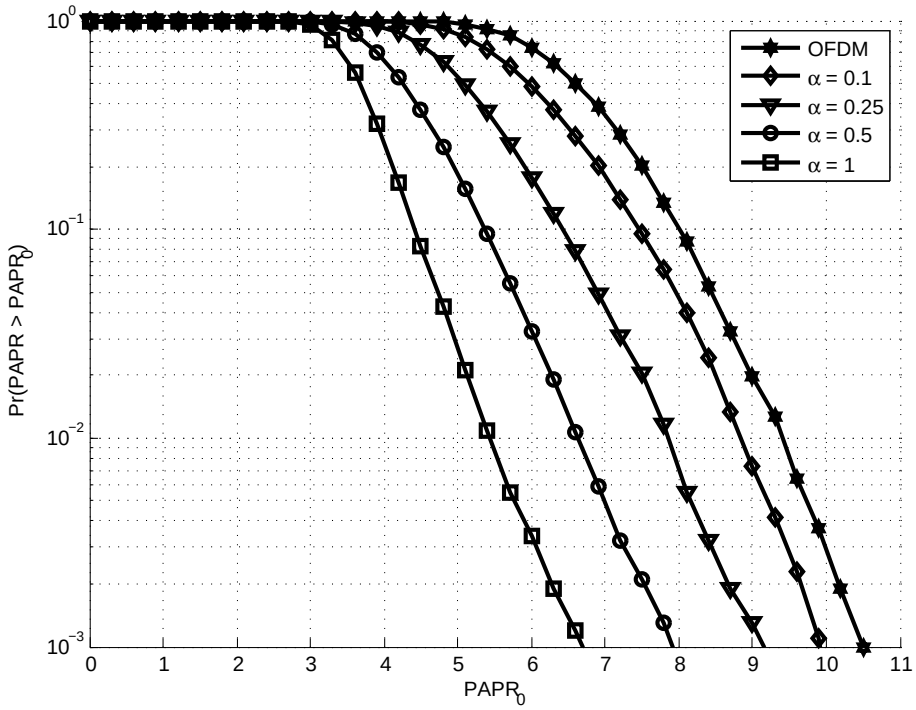

Figure 4.7 PAPR performance for 4-QAM when $\lambda = 0.5$.

The performance of the proposed suppressing alignment scheme in reducing both the OOB power leakage and PAPR depends on the PDP of the wireless channel. The results presented so far are based on a uniform PDP. Thus, to quantify the impact of the PDP of the wireless channel, we also evaluate the performance under an exponentially decaying PDP with a decaying constant[1] set to 2. The effect of the PDP on the OOB power leakage reduction is shown in Figure 4.8 for 16-QAM. As evident in Figure 4.8, there is a noticeable degradation in the OOB power leakage reduction when the channel has an exponentially decaying PDP. A similar outcome is expected for the PAPR performance as shown in Figure 4.9. These results show that a uniform PDP gives more degrees of freedom in suppressing the OOB power leakage compared to that of an exponentially decaying PDP.

[1] $\frac{\mathbb{E}[h_l]}{\mathbb{E}[h_0]} = \exp(\frac{-l}{2}),\ l = 0, ..., L$.

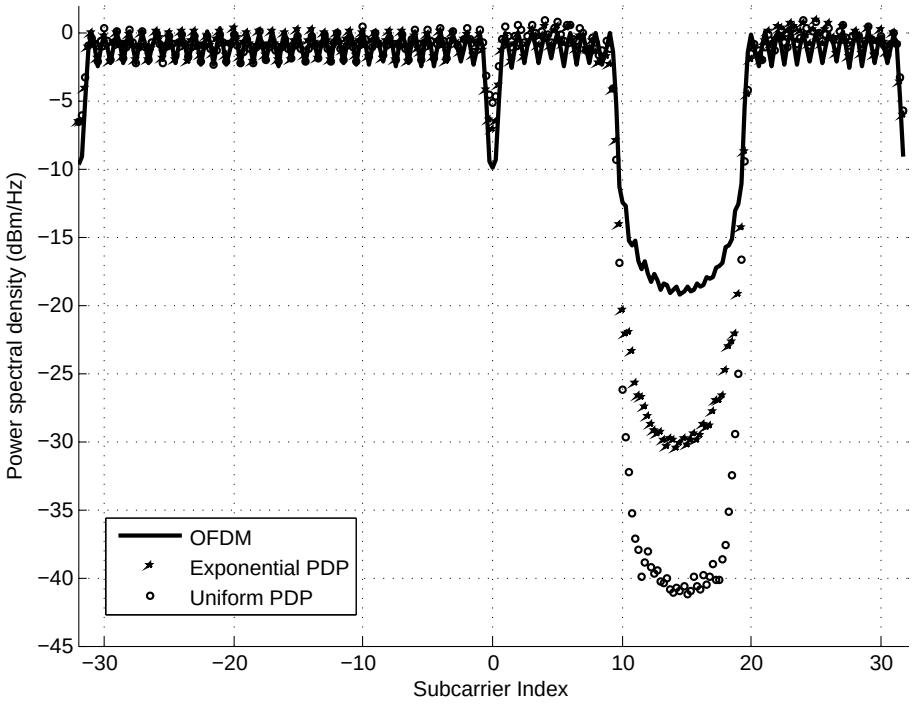

Figure 4.8 Power spectral density for 16-QAM for $\alpha = 0.25, \lambda = 0$.

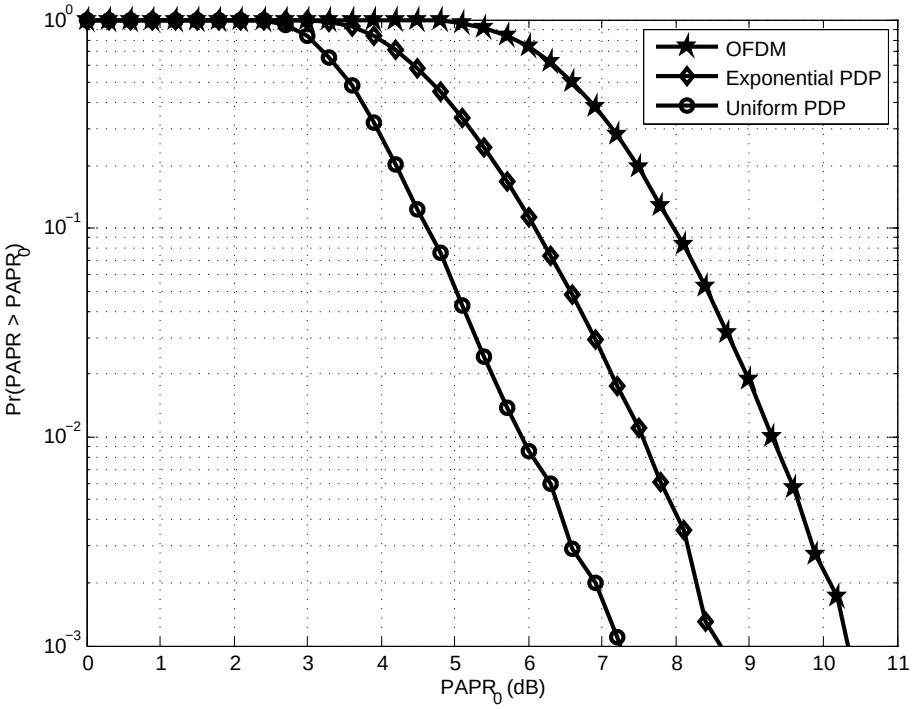

Figure 4.9 PAPR performance for 16-QAM for $\alpha = 0.25, \lambda = 1$.

4.5.2 Imperfect Channel State Information

In a practical environment, the assumption of perfect channel knowledge might not be valid. Therefore, in this subsection we evaluate the performance of the proposed algorithm when the transmitter has imperfect CSI. The channel is estimated at the receiver and the CSI is fed back to the transmitter. The transmitter then uses this CSI to generate the suppressing signal $\mathbf{c} = \mathbf{Ps}$. To evaluate the impact of channel estimation errors, we assume that the channel used at the transmitter is different than the real channel that the signal is transmitted through. We quantify the error in channel estimation by the mean square error (MSE) defined as

$$\text{MSE} = \mathbb{E}[\frac{1}{N}\sum_{k=1}^{N}|\hat{H}(k) - H(k)|^2] \ , \tag{4.18}$$

where k is the subcarrier index and $\hat{H}(k)$ is the erroneous channel given by

$$\hat{H}(k) = H(k) + e(k) \ , \tag{4.19}$$

where the estimation error $e(k)$ is modeled as a complex Gaussian random variable with zero mean and variance σ_e^2 equal to the MSE in (4.18). This simple model has previously been used in [72] to roughly evaluate the impact of imperfect CSI.

The received signal after CP removal and DFT operation is given by (4.5), where the precoding matrix $\mathbf{P}$ is designed based on knowledge of the channel at the transmitter. If the channel communicated back to the transmitter by the receiver is erroneous, then $\mathbf{P}$ is designed based on $\hat{\mathbf{H}}$ as opposed to the true channel $\mathbf{H}$. Therefore, the second term in (4.5) would not vanish, i.e., (4.6) is not true any more. This effectively means that the suppressing signal leaks into the data part of the OFDM symbol instead of precisely being aligned with the CP duration. Nevertheless, the erroneous channel information does not effect the OOB power leakage and PAPR reduction performance of the proposed method, since the suppressing signal is still designed based on (4.12) or (4.17).

Using the simplified model above, we conducted Monte Carlo simulations to assess the impact of this leakage on the BER performance of the proposed algorithm for different values of SNR as shown in Figure 4.11. Our simulations are bench-marked against the error performance of plain OFDM under the same noisy channel estimation. As observed in Figure 4.11, the error performance of the suppressing alignment algorithm is identical to that of standard OFDM under channel estimation errors. This can be explained by looking at Figure 4.10. There, the average power leakage of the suppressing signal into the data part of the received OFDM symbol, defined as

$$\mathbf{Q} = \mathbb{E}[\|\mathbf{BHPs}\|_2^2] \ , \tag{4.20}$$

is plotted against the MSE of the channel for different values of α. In Figure 4.10, the leaked power is at least 8 dB less than the channel MSE when $\alpha = 0.25$. Essentially, the noisy channel dominates the error performance. As such, no degradation in the BER is observed as shown in Figure 4.11 when $\alpha = 0.25$.

4.6 Conclusion

In this chapter, we have proposed an approach called *suppressing alignment* that generates a suppressing signal to jointly reduce the OOB power leakage and PAPR of OFDM-based systems. The main advantage of the proposed approach is that it does not reduce the spectral efficiency as it exploits the inherent redundancy in OFDM provided by the CP. We have also shown that the suppressing signal can be constructed in such a way that it does not create any interference to the information data carried in the OFDM symbol. In particular, by utilizing the wireless channel, the suppressing signal is aligned with the CP duration at the receiver, effectively creating an interference-free transmission with a BER performance similar to legacy OFDM without requiring any change in the receiver structure. The effectiveness of the proposed approach in obtaining remarkable reduction in both the OOB power leakage and PAPR is shown with computer simulations. We showed the performance trade-off between the OOB power leakage reduction and PAPR

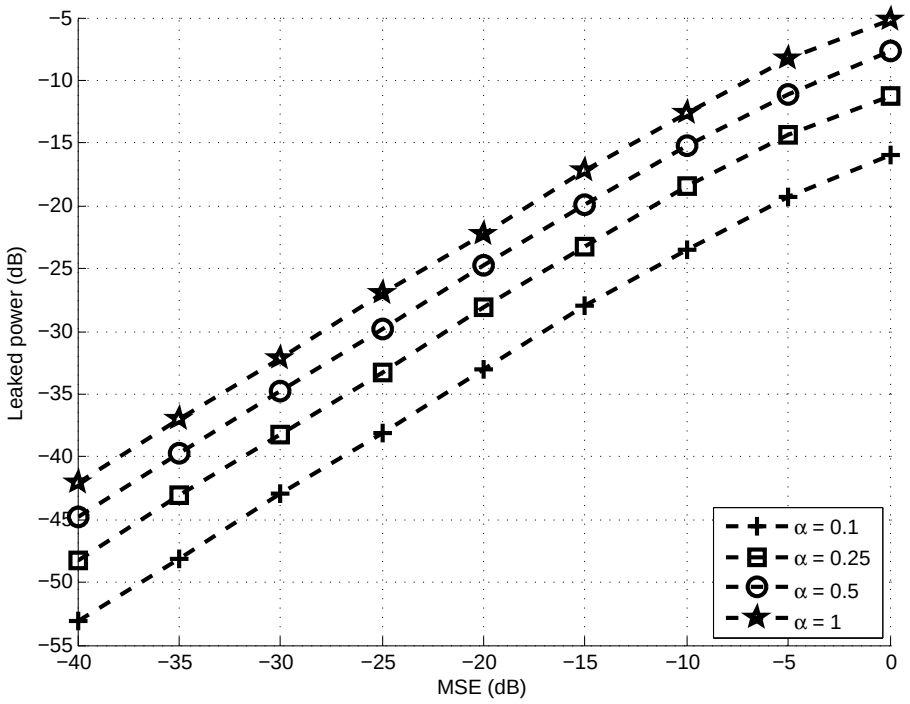

Figure 4.10 Leaked power of the suppressing signal under imperfect CSI, $\lambda = 0.5$.

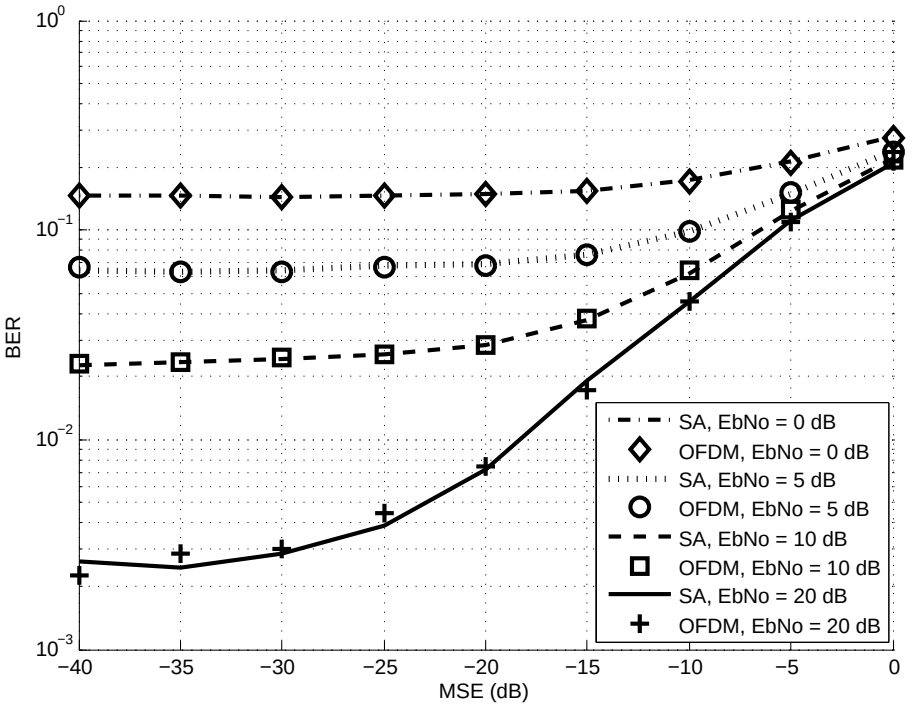

Figure 4.11 BER performance under imperfect CSI, $\lambda = 0.5,\ \alpha = 0.25$.

reduction where both can flexibly be controlled though an adaptation parameter. Furthermore, we investigated the impact of imperfect CSI on the error performance of the proposed approach. The simulation results show no degradation in the BER performance of the proposed approach compared to legacy OFDM under the same noisy channel errors.

CHAPTER 5

TWO ERROR VECTOR MAGNITUDE COMPLIANT PRECODERS FOR OUT-OF-BAND POWER LEAKAGE REDUCTION IN OFDM BASED SYSTEMS

5.1 Introduction

Out of all the reported OOB reduction algorithms in the literature, precoding schemes are the most effective in achieving significant suppression of the OFDM spectral emissions. However, since precoding typically changes the transmitter structure of OFDM, side information regarding the precoder needs to be sent to the receiver for it to be able to decode the information symbols. The side information is usually large, as the precoder is typically a full matrix with dimensions as large as the transmitted data itself. This can potentially result in huge reduction in the transmission rate, especially if the precoder information needs to be transmitted frequently, as usually the case in cognitive radio scenarios where the spectral resources change regularly making it necessary to recalculate the precoder.

In this chapter, we also consider precoding for reducing the OFDM spectral sidelobes. However, we target the design of precoders where the receiver does not need to know any information about the precoding done at the transmitter to be able to recover the information symbols. Such a design can significantly improve the spectral efficiency of the system as no resources are wasted in sending any side information to the receiver. The receiver can usually decode the information symbols with acceptable error probabilities if the precoded data falls within particular constellation errors [73], typically specified by the OFDM standard in the form of an EVM limit. Therefore, our focus in this chapter is on precoders that minimize the OOB emissions under a hard constraint on a specified EVM which is typically provided as a root mean square (RMS) value [74].

The rest of the chapter is organized as follows. In Section 5.2, the system model is introduced. In Section 5.3, we present the two EVM compliant precoders for reducing the OOB power

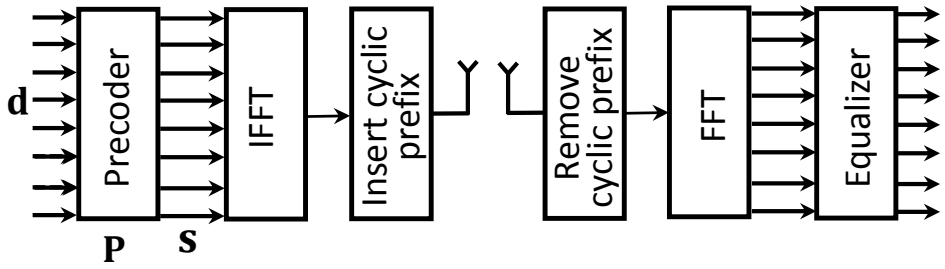

Figure 5.1 System model.

leakage of OFDM. The numerical results are provided in Section 5.4 and finally the conclusion is given in Section 5.5.

In this chapter, $\mathbf{I}_K$ is the $K \times K$ identity matrix. The transpose and conjugate transpose are denoted by $(\cdot)^{\mathrm{T}}$ and $(\cdot)^{\mathrm{H}}$, respectively. $\|\cdot\|_2$ denotes the 2-norm while the Frobenius norm is denoted by $\|\cdot\|_{\mathrm{F}}$. The expectation operator is denoted by $\mathbb{E}[\cdot]$ while the trace of a matrix is denoted by $\mathrm{Tr}\{\cdot\}$.

5.2 System Model

We consider an OFDM system with K subcarriers where a precoder is introduced in the transmitter for the purpose of reducing the spectral emissions of the signal as shown in Figure 5.1. The transmitter in this case is different than a legacy OFDM transmitter due to the introduction of the precoder block. The purpose of the precoder block is to pre-process the data stream $\mathbf{d}$ by a $K \times K$ matrix $\mathbf{P}$ with the objective of generating new transmission data with better spectral emissions. The resulting data vector $\mathbf{s}$ after precoding is expressed in a matrix form as

$$\mathbf{s} = \mathbf{P}\mathbf{d} \ . \tag{5.1}$$

The precoder vector $\mathbf{s}$ is then used to modulate the available K subcarriers using the DFT block. After DFT, the resulting parallel stream is converted to a serial stream and a CP of length larger than the maximum excess delay of the channel is appended to the start of the serial stream in order

to mitigate the detrimental effects of ISI. The generated OFDM signal is then written as

$$x(t) = \sum_{k=0}^{K-1} s_k e^{j2\pi \frac{k}{T_s} t} R_c(t) \ , \tag{5.2}$$

where T_s is the useful duration of the OFDM symbol, s_k is the kth element of the vector $\mathbf{s}$ and $R_c(t)$ is a rectangular window function defined as

$$R_c(t) = \begin{cases} 1 \ , & \frac{-T}{2} < t < \frac{T}{2} \\ 0 \ , & \text{otherwise} \end{cases} \tag{5.3}$$

and $T = T_s + T_{\text{cp}}$, where T_{cp} is the CP duration. The CP is removed at the receiver and the remaining data is fed to the inverse discrete Fourier transformation (IDFT) block to generate an estimate of the precoded vector $\mathbf{s}$, which is then passed to the detector for direct mapping to the original quadrature amplitude modulation (QAM) symbols.

The OOB power leakage contribution of the kth subcarrier at some frequency f outside the designated band of transmission is found by taking the Fourier transform on the rectangular windowed kth subcarrier as follows:

$$a_k(f) = \frac{1}{T_s + T_{\text{cp}}} \int_{-\infty}^{\infty} R_c(t) e^{j\frac{2\pi k}{T_s} t} e^{-j2\pi f t} \, dt = \text{sinc}\left(T(f - \frac{k}{T_s}) \right) \ , \tag{5.4}$$

accordingly, the total OOB leakage from all subcarriers modulated by the vector $\mathbf{s}$ in M discrete frequency locations $f_m \in \{f_0, f_1, ..., f_{\text{M}-1}\}$ is written in a matrix form as

$$\boldsymbol{\mathcal{F}_s} = \mathbf{As} = \mathbf{APd} \ , \tag{5.5}$$

where $\mathbf{A}$ is an $M \times K$ matrix with entries $a_k(f_m)$ representing the OOB power leakage from the kth subcarrier at some discrete frequency f_m outside the transmission band. The average OOB

power leakage can thus be expressed as

$$\begin{aligned}\boldsymbol{\mathcal{S}}_{\boldsymbol{a}} = \mathbb{E}\{\|\mathbf{APd}\|_2^2\} = \mathrm{Tr}\{\mathbb{E}\{\mathbf{APdd}^{\mathrm{H}}\mathbf{P}^{\mathrm{H}}\mathbf{A}^{\mathrm{H}}\}\} = \\ \mathrm{Tr}\{\mathbf{APP}^{\mathrm{H}}\mathbf{A}^{\mathrm{H}}\} = \mathrm{Tr}\{\mathbf{P}^{\mathrm{H}}\mathbf{A}^{\mathrm{H}}\mathbf{AP}\} \ .\end{aligned} \tag{5.6}$$

The last result in (5.6) is due to $\mathbb{E}\{\mathbf{dd}^{\mathrm{H}}\} = \mathbf{I}_K$. Since $\mathrm{Tr}\{\mathbf{P}^{\mathrm{H}}\mathbf{A}^{\mathrm{H}}\mathbf{AP}\} = \|\mathbf{AP}\|_{\mathrm{F}}^2$, therefore minimizing the average OOB power leakage corresponds to minimizing the Frobenius norm of the matrix $\mathbf{AP}$.

5.3 Precoding Schemes

In this section, we design two precoders, a full rate EVM compliant precoder which we will refer to as precoder A, and another EVM compliant precoder with free subcarriers which we refer to as precoder B. First we start by presenting precoder A.

5.3.1 Precoder A

We start by designing the precoder $\mathbf{P}$ that minimizes the average spectrum in (5.6) while satisfying a desired EVM constraint. The average EVM measures the error between the ideal constellation vector $\mathbf{d}$ and the constellation vector that is actually transmitted $\mathbf{s}$, and is defined as

$$\mathrm{EVM} = \sqrt{\frac{\mathbb{E}\{\|\mathbf{d}-\mathbf{s}\|_2^2\}}{\mathbb{E}\{\|\mathbf{d}\|_2^2\}}} = \sqrt{\frac{\mathbb{E}\{\|(\mathbf{I}_K-\mathbf{P})\mathbf{d}\|_2^2\}}{K}} \ . \tag{5.7}$$

As stated above, the goal here is to design the precoder $\mathbf{P}$ under the constraint of a given EVM. Therefore the desired precoder $\mathbf{P}$ is the solution to the following optimization problem

$$\begin{aligned}&\mathbf{P} = \arg\min_{\mathbf{P}} \ \mathrm{Tr}\{\mathbf{P}^{\mathrm{H}}\mathbf{A}^{\mathrm{H}}\mathbf{AP}\} \\ &\text{subject to} \ \ \mathbb{E}\{\|(\mathbf{I}_K-\mathbf{P})\mathbf{d}\|_2^2\} \leq \alpha \ ,\end{aligned} \tag{5.8}$$

where α is given by

$$\alpha = (\mathrm{EVM}_{\max})^2 K. \tag{5.9}$$

The maximum EVM, i.e., $\mathrm{EVM}_{\max}$ is usually specified by the wireless standard [75]. To get rid of the data dependency of the constraint in (5.8), we can further expand it as

$$\begin{aligned}\mathbb{E}\{\|(\mathbf{I}_K - \mathbf{P})\mathbf{d}\|_2^2\} &= \mathrm{Tr}\{\mathbb{E}\{(\mathbf{I}_K - \mathbf{P})\mathbf{d}\mathbf{d}^{\mathrm{H}}(\mathbf{I}_K - \mathbf{P})^{\mathrm{H}}\}\} \\ &= \mathrm{Tr}\{(\mathbf{I}_K - \mathbf{P})(\mathbf{I}_K - \mathbf{P})^{\mathrm{H}}\} = K - 2\mathrm{Tr}\{\mathbf{P}\} + \mathrm{Tr}\{\mathbf{P}\mathbf{P}^{\mathrm{H}}\} \leq \alpha\ . \end{aligned} \tag{5.10}$$

Due to the symmetry of the rectangular window function in (5.3), the OOB power leakage matrix $\mathbf{A}$ is real. Therefore the precoder $\mathbf{P}$ is also real and $\mathbf{P}^{\mathrm{H}} = \mathbf{P}^T$, $\mathbf{A}^{\mathrm{H}} = \mathbf{A}^{\mathrm{T}}$. Now we can re-write the problem in (5.8) as

$$\begin{aligned}&\mathbf{P} = \arg\min_{\mathbf{P}}\ \mathrm{Tr}\{\mathbf{P}^{\mathrm{T}}\mathbf{A}^{\mathrm{T}}\mathbf{A}\mathbf{P}\} \\ &\text{subject to}\ \ K - 2\mathrm{Tr}\{\mathbf{P}\} + \mathrm{Tr}\{\mathbf{P}\mathbf{P}^{\mathrm{T}}\} \leq \alpha\ .\end{aligned} \tag{5.11}$$

In order to solve the optimization problem (5.11), let us define

$$\phi = \mathrm{Tr}\{\mathbf{P}^{\mathrm{T}}\mathbf{A}^{\mathrm{T}}\mathbf{A}\mathbf{P}\},\ \psi = K - 2\mathrm{Tr}\{\mathbf{P}\} + \mathrm{Tr}\{\mathbf{P}\mathbf{P}^{\mathrm{T}}\} - \alpha\ . \tag{5.12}$$

Using the Lagrange multipliers method, we seek $\lambda \in \mathbb{R}$ such that

$$\nabla_{\mathbf{P}}\phi + \lambda\nabla_{\mathbf{P}}\psi = 0\ , \tag{5.13}$$

where $\nabla_{\mathbf{P}}$ is the gradient operator with respect to the matrix $\mathbf{P}$ and $\lambda > 0$ is the Lagrange multiplier. From [76], we have the following three properties regarding the derivative of the trace with respect to a matrix $\mathbf{X}$

$$\frac{\partial}{\partial \mathbf{X}}\mathrm{Tr}\{\mathbf{X}\} = \mathbf{I}\ , \tag{5.14}$$

$$\frac{\partial}{\partial \mathbf{X}} \mathrm{Tr}\{\mathbf{X}^T \mathbf{Y} \mathbf{X}\} = \mathbf{Y}\mathbf{X} + \mathbf{Y}^T \mathbf{X} \ , \tag{5.15}$$

and

$$\frac{\partial}{\partial \mathbf{X}} \mathrm{Tr}\{\mathbf{X}^T \mathbf{X}\} = 2\mathbf{X} \ . \tag{5.16}$$

Let $\mathbf{X} = \mathbf{P}$ and $\mathbf{Y} = \mathbf{A}^T\mathbf{A}$, therefore

$$\nabla_{\mathbf{P}} \phi + \lambda \nabla_{\mathbf{P}} \psi = \frac{\partial}{\partial \mathbf{X}} \mathrm{Tr}\{\mathbf{X}^T \mathbf{Y} \mathbf{X}\} + \lambda \frac{\partial}{\partial \mathbf{X}} (K - 2\mathrm{Tr}\{\mathbf{X}\} + \mathrm{Tr}\{\mathbf{X}\mathbf{X}^T\} - \alpha) = 0 \ , \tag{5.17}$$

using the derivative properties of the trace above, we obtain

$$\mathbf{Y}\mathbf{X} + \mathbf{Y}^T\mathbf{X} + \lambda(-2\mathbf{I} + 2\mathbf{X}) = 0 \ , \tag{5.18}$$

therefore if we substitute for $\mathbf{X}$ and $\mathbf{Y}$ we get

$$\mathbf{A}^T\mathbf{A}\mathbf{P} + \mathbf{A}^T\mathbf{A}\mathbf{P} + 2\lambda(\mathbf{P} - \mathbf{I}) = 2\mathbf{A}^T\mathbf{A}\mathbf{P} + 2\lambda(\mathbf{P} - \mathbf{I}) = 2\mathbf{A}^T\mathbf{A}\mathbf{P} + 2\lambda(\mathbf{P} - \mathbf{I}) = 0 \ , \tag{5.19}$$

Hence,

$$\mathbf{P} = \left(\frac{1}{\lambda} \mathbf{A}^T\mathbf{A} + \mathbf{I} \right)^{-1} \ . \tag{5.20}$$

For a given α or an EVM value as defined in (5.9), λ is found such that it satisfies the constraint in (5.11). First, let $\mathbf{X} = \mathbf{A}^T\mathbf{A}$, clearly $\mathbf{X}$ is a symmetric matrix which makes $\mathbf{P}$ also symmetric. Furthermore, let $\gamma_j(\mathbf{Y})$ be the eigenvalues of any symmetric matrix $\mathbf{Y}$. Therefore, since $(\mathbf{I} - \mathbf{P})^T = \mathbf{I} - \mathbf{P}$ because $\mathbf{P}$ is symmetric, we have

$$\mathrm{Tr}\{(\mathbf{I} - \mathbf{P})(\mathbf{I} - \mathbf{P})^T\} = \sum_j \gamma_j^2(\mathbf{I} - \mathbf{P}) \ . \tag{5.21}$$

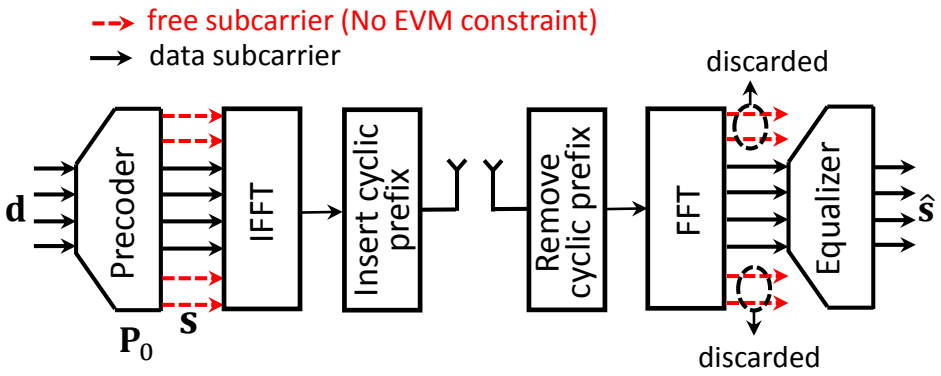

Figure 5.2 System model for precoder B.

Since $\gamma_j(\mathbf{I}-\mathbf{P}) = 1-\gamma_j(\mathbf{P}) = 1-\frac{1}{\frac{1}{\lambda}\gamma_j(\mathbf{X})+1}$, λ is the solution to the following

$$\sum_j \big(1-\frac{1}{\frac{1}{\lambda}\gamma_j(\mathbf{X})+1}\big)^2 = \alpha \ . \tag{5.22}$$

We note here that once λ is determined, the precoder $\mathbf{P}$ is fixed and is independent of the data symbols for a given spectral occupancy. Moreover, since the precoder $\mathbf{P}$ produces symbols with EVM that falls within limits predetermined by the OFDM standard, the receiver will have satisfactory BER performance without changing the receiver structure of classical OFDM if the transmitter uses error-correction codes [73]. It is worth noting that the EVM compliant precoder in (5.20) is a full rate precoder that does not reduce the transmission rate.

5.3.2 Precoder B

In this subsection, we design another precoder that enhances the OOB leakage performance of precoder A, albeit at the expense of some reduction in the system transmission rate, by utilizing some subcarriers at the edges of the transmission band as free subcarriers as shown in Figure 5.2. The weights of the free carriers are calculated as a function of the information data. This choice helps in making the precoder independent of the information data as will be shown below. The difference between this precoder and precoder A is that in addition to using the degrees of freedom of the allowed constellation error, i.e., EVM, it also uses the free carriers to improve the reduction of the OOB leakage.

Let the total number of subcarriers K be partitioned into N_{d} data subcarriers and N_{r} free subcarriers where $K = N_{\mathrm{d}} + N_{\mathrm{r}}$. Also, let us define a $K \times N_d$ matrix $\mathbf{B}$ containing the N_{d} columns of the $K \times K$ identity matrix $\mathbf{I}_K$ corresponding to the data subcarriers and a $K \times N_{\mathrm{r}}$ matrix $\mathbf{C}$ containing the N_r columns of the $K \times K$ identity matrix corresponding to the free subcarriers. Both $\mathbf{B}$ and $\mathbf{C}$ are subcarrier selection matrices. We can now write the precoded vector $\mathbf{s}$ as

$$\mathbf{s} = \mathbf{B}\mathbf{d} + \mathbf{w} \ , \tag{5.23}$$

where $\mathbf{d} = [d_1, d_2, ..., d_{N_d}]$ is an $N_d \times 1$ information data vector and $\mathbf{w} = [w_1, w_2, ..., w_K]$ is an $K \times 1$ distortion vector which will be designed to control the spectral emissions of the precoded data in $\mathbf{s}$ where some of the elements of $\mathbf{w}$ act as free carriers. For example, if 4 free subcarriers are allocated with 2 on each side of the transmission band, then $\mathbf{s} = [w_1, w_2, d_1 + w_3, ..., d_{N_d} + w_{K-2}, w_{K-1}, w_K]$. Note that the weights of the free carriers are exactly the corresponding elements in the vector $\mathbf{w}$. Moreover, the information data is also distorted, however and as mentioned before, this distortion will be controlled to satisfy a given EVM.

In this work, we choose $\mathbf{w}$ as a linear combination of the information data in $\mathbf{d}$, in particular we design $\mathbf{w}$ as

$$\mathbf{w} = \mathbf{G}\mathbf{d} \ . \tag{5.24}$$

(5.24) creates free carriers that are a linear combination of the data. The precoded vector $\mathbf{s}$ in (5.23) is therefore written as

$$\mathbf{s} = \mathbf{B}\mathbf{d} + \mathbf{G}\mathbf{d} = \underbrace{(\mathbf{B} + \mathbf{G})}_{\mathbf{P_0}}\mathbf{d} \ , \tag{5.25}$$

where $\mathbf{P}_0$ is the desired precoder. However, since $\mathbf{B}$ is known, finding the precoder $\mathbf{P}_0$ is equivalent to finding the matrix $\mathbf{G}$. The main objective in the construction of the precoder $\mathbf{G}$ is to reduce the OOB power leakage of the transmitted signal. However, in addition to that, we have two additional goals: first, the precoded data should satisfy an acceptable EVM value specified by the OFDM

standard. Second, the power of the free carriers, which are calculated as a linear combination of the data as a result of (5.24), should be controlled in a such away that it's only a fraction of the power consumed by the data subcarriers. There are good reasons in keeping the power allocated to the free carriers small. First, the free subcarriers are dummy subcarriers that do not carry any useful information, they are only used for the purpose of reducing the spectral emissions of the transmitted signal. Second, allocating too much power to the free subcarriers increases the PAPR of the signal, which might lead to a spectral regrowth problem, specially if the peak power of the signal drove the PA into its non-linear region.

Since the subcarriers are divided into data subcarriers and free subcarriers, the EVM is a function of only the data subcarriers. The free subcarriers are excluded from the EVM calculation since they do not carry any useful information. Using the subcarrier selection matrix $\mathbf{B}$ defined above, the average EVM constraint can be written as

$$\mathbb{E}\{\|\mathbf{d}-\mathbf{B}^{\mathrm{T}}\mathbf{s}\|_2^2\} = \mathbb{E}\{\|(\mathbf{I}-\mathbf{B}^{\mathrm{T}}(\mathbf{B}+\mathbf{G}))\mathbf{d}\|_2^2\} \leq \alpha \ , \tag{5.26}$$

and as what we did in (5.10), this can be further expanded to

$$\begin{aligned}\mathrm{Tr}\{(\mathbf{I}_{\mathrm{N_d}}-\mathbf{B}^{\mathrm{T}}(\mathbf{B}+\mathbf{G}))(\mathbf{I}_{N_d}-\mathbf{B}^{\mathrm{T}}(\mathbf{B}+\mathbf{G}))^{\mathrm{T}}\} \\ = \|\mathbf{I}_{N_d}-\mathbf{B}^{\mathrm{T}}(\mathbf{B}+\mathbf{G})\|_{\mathrm{F}}^2 \leq \alpha \ ,\end{aligned} \tag{5.27}$$

As mentioned above, we also constrain the mean power of the free subcarriers to be below a certain level. This constraint is written as

$$\mathbb{E}\{\|\mathbf{C}^{\mathrm{T}}(\mathbf{B}+\mathbf{G})\mathbf{d}\|_2^2\} \leq \beta \ , \tag{5.28}$$

where $\mathbf{C}^{\mathrm{T}}$ is a selection matrix for the free subcarriers and β is the power overhead defined as the ratio between the power consumed by the free subcarriers and the power used by the data subcarriers which is assumed to be 1. Since the information data in $\mathbf{d}$ is i.i.d with zero mean and unit variance, (5.28) is therefore independent of the information data, Hence, similar to the EVM

constraint above, (5.28) is expanded as

$$\|\mathbf{C}^T(\mathbf{B}+\mathbf{G})\|_{\mathrm{F}}^2 \leq \beta \ . \tag{5.29}$$

The average OOB power leakage expression of the precoded data in (5.25) is similar to the one in (5.6) except that the precoder is different here, and is written as

$$\boldsymbol{\mathcal{S}}_b = \mathbb{E}\{\|\mathbf{A}(\mathbf{B}+\mathbf{G})\mathbf{d}\|_2^2\} = \|\mathbf{A}(\mathbf{B}+\mathbf{G})\|_{\mathrm{F}}^2 \ . \tag{5.30}$$

To minimize the OOB power leakage in (5.30) subject to the constraints in (5.27) and (5.29), we formulate the optimization problem as follows

$$\begin{aligned} &\mathbf{P} = \arg\min_{\mathbf{G}} \ \|\mathbf{A}(\mathbf{B}+\mathbf{G})\|_{\mathrm{F}}^2 \\ &\text{subject to} \ \ \|\mathbf{I}_{N_d} - \mathbf{B}^{\mathbf{T}}(\mathbf{B}+\mathbf{G})\|_{\mathrm{F}}^2 \leq \alpha \\ &\|\mathbf{C}^T(\mathbf{B}+\mathbf{G})\|_{\mathrm{F}}^2 \leq \beta \ , \end{aligned} \tag{5.31}$$

to the best of our knowledge, there is no closed-form solution to (5.31). However, the problem is convex and can be solved numerically using any optimization package. In this work, we use YALMIP [70] with MOSEK [71] as the underlying solver, both of which are easily integrated with MATLAB. We would like to note that although the precoder in (5.31) does not have a closed-form solution, it can be solved off-line only once and used for all incoming OFDM symbols as long as the spectral occupancy does not change.

5.4 Numerical Results

5.4.1 Precoder A Performance

We first evaluate the performance of precoder A. In all simulation results, we adopt the OFDM parameters of the 3GPP LTE standard with $K = 300$ subcarriers, $T_s = \frac{1}{15}$ ms and $T_{\mathrm{cp}} = \frac{9}{128}$ ms. The OOB power leakage is estimated by generating 10^3 random 4-QAM symbols.

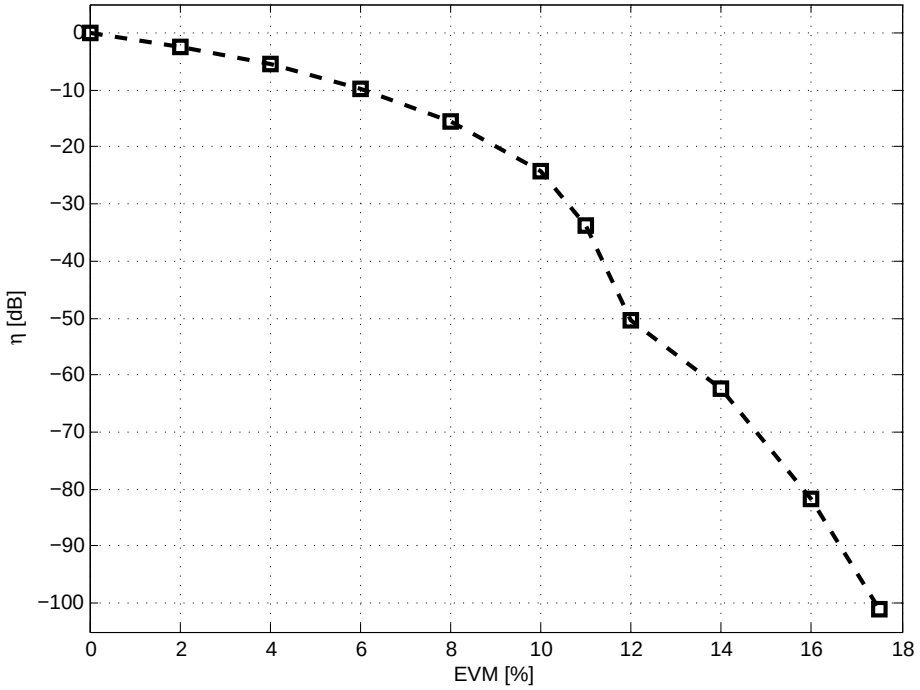

Figure 5.3 EVM vs. mean OOB power leakage reduction.

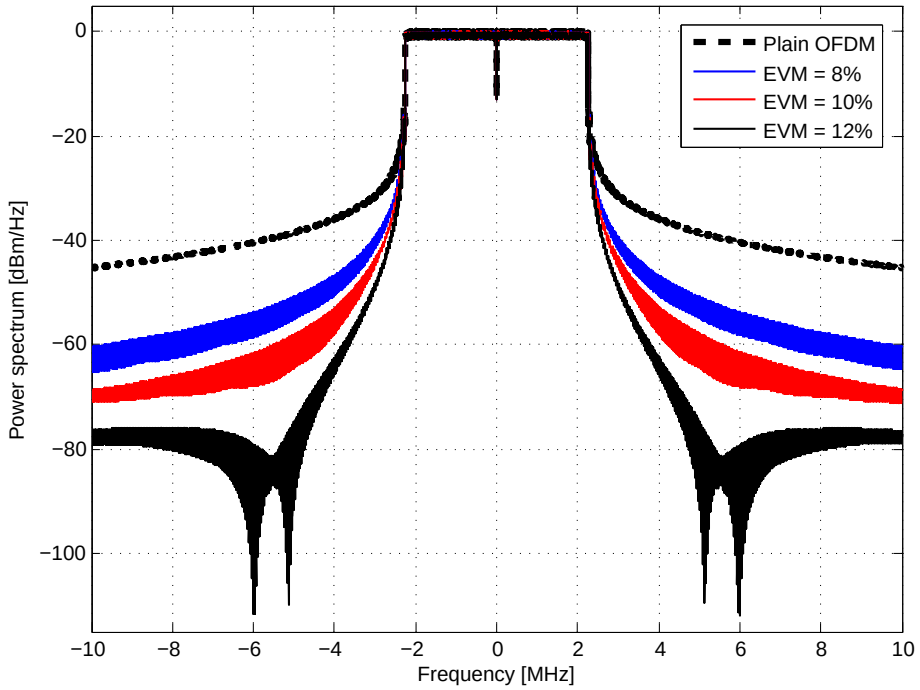

Figure 5.4 OOB reduction performance of precoder A.

In Figure 5.3, we show the average OOB power leakage reduction for different EVM values in terms of the reduction factor η defined as the ratio of the OOB power leakage of the precoded data to the OOB power leakage of the uncoded data

$$\eta = \frac{\|\mathbf{AP}\|_F^2}{\|\mathbf{A}\|_F^2} \tag{5.32}$$

Figure 5.3 shows that as the allowed EVM tolerance increases, more reduction in the OOB power leakage is achieved. We remark here that the maximum allowed EVM for 4-QAM symbols is 17.5% as specified by the 3GPP LTE standard. At this EVM value, the proposed precoder can result in an average OOB power leakage reduction of more than 100 dB. However, it's not practical to use all the maximum allowed EVM tolerance just to reduce OOB emissions. Some room should be left for other impairments such as the distortion introduced by the nonlinearity of the PA. Nonetheless, remarkable OOB leakage reduction can still be achieved even if some EVM margin is allocated for other impairments. For example, a reduction of 18 dB is achieved at an EVM value of 8% while an allowed EVM of 10% reduces the OOB leakage by more than 26 dB. The PSD of the transmitted signal for different EVM values is shown in Figure 5.4 along with that of a plain OFDM signal. We select 8 discrete frequencies, $f_m = \{\pm 6100 \pm 1, \pm 5100 \pm 1\}$, where the power spectrum is to be minimized by the precoder (5.20). Our choice of adjacent frequencies comes from the fact that positioning pairs of frequencies close to each other significantly improves the OOB power leakage reduction of the precoder, which has also been observed previously in [1]. As expected, the spectral suppression of the precoder improves as the allowed EVM margin increases. An EVM tolerance of 12%, which still leaves enough head room for other impairments, results in remarkable OOB power leakage reduction.

The spectral suppression performance of precoder A with respect to other state of the art precoders in [1] and [2] is shown in Figure 5.5. For a fair comparison, we fixed the EVM value for all precoders at 12% with 4-QAM symbols employed in the transmission. In [2], three precoders are proposed that make N-continuous OFDM signals compatible with the EVM requirements specified by the OFDM standard. N-continuous OFDM signals are originally introduced in [31] to improve

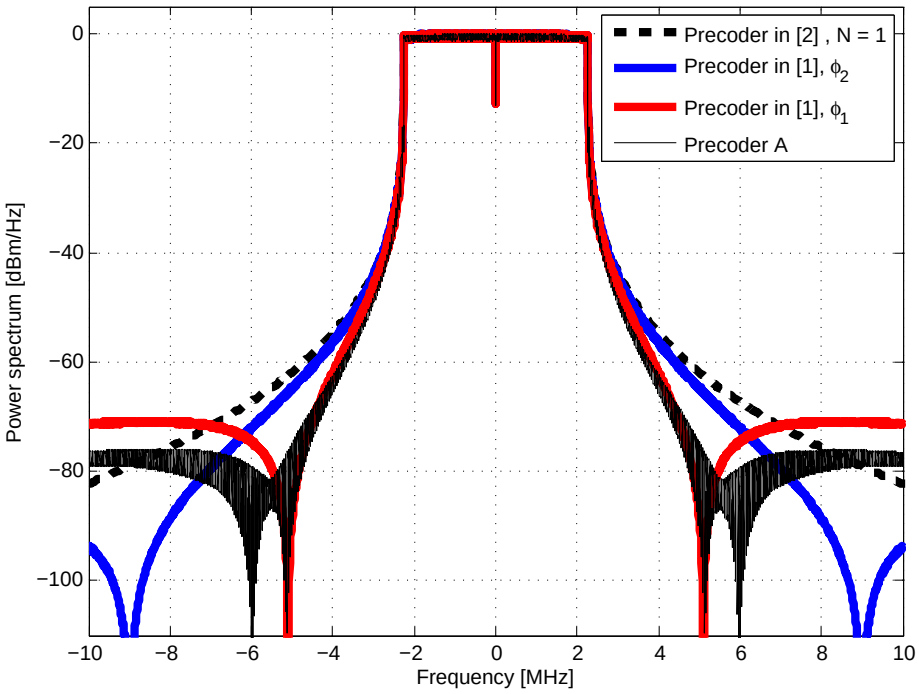

Figure 5.5 Performance of precoder A against the precoders in [1] and [2]; EVM = 12% for 4-QAM.

the spectrum emissions of classical OFDM signals. Out of the three precoders in [2], we choose precoder (21) which has the best suppression performance among all three. Furthermore, we choose a continuity order of $N = 1$ which provides the best spectral suppression performance compared to other orders of continuity for the given number of subcarriers $K = 300$ and the specified EVM= 12%. The reader can refer to [2] for the details of choosing the parameter values of precoder (21) in [2]. Results in Figure 5.5 clearly show the superiority of precoder A over the precoder (21) in [2] (dashed line) with regard to the OOB power leakage reduction.

We also compare the suppression performance of precoder A to the nullspace projection precoder in [1]. The projection precoder has an EVM= $\sqrt{M/K}$, where M is the number of discrete frequencies where spectral nulls (notches) are desired. Therefore for this projection precoder to create signals with EVM = 12%, M is calculated to be around 4.32. That means, at most 4 discrete notch frequencies can be selected in the OOB region in order to minimize the spectrum. To show the performance of the projection precoder, We select two sets of 4 discrete notch frequencies: $\phi_1 = \{\pm 5100 \pm 1\}$ which is close to the band of transmission and $\phi_2 = \{\pm 8999 \pm 1\}$ in the far region,

away from the transmission band. Over the region close to the transmission band, the OOB power leakage reduction performance of precoder A is identical to that of the projection precoder with notching frequencies ϕ_1, but better than the projection precoder with nothching frequencies ϕ_2 as shown in Figure 5.5. As we move away from the transmission band, precoder A achieves better suppression compared to the projection precoder with notching frequencies ϕ_1. The performance of precoder A is inferior to the projection precoder with notching frequencies ϕ_2 only in the far region. Another advantage of precoder A over the projection precoder [1] is that there is no restriction on how many frequencies can be chosen in the OOB region to minimize power spectrum. This is clearly not the case for the projection precoder as the number of notch frequencies is dependent on the number of subcarriers and the allowed EVM. No such dependency exists for precoder A, and therefore its parameters can be adapted more flexibly to achieve the best OOB power leakage performance.

5.4.2 Precoder B Performance

First, we show the constellation of the transmitted symbols resulting from precoder B in Figure 5.6. Since there is no restriction on the distortion exerted on the free subcarriers, the symbols (not necessarily 4-QAM) transmitted over them are scattered in the entire constellation. On the other hand, the distortion on the data subcarriers is contrained to produce an EVM = 8%. As such, the precoded data subcarriers are slightly distorted compared to the ideal 4-QAM constellations as shown in Figure 5.6. It is this degree of freedom in distorting the free subcarriers that improves the spectral suppression performance of precoder B over precoder A as will be shown in the results below. In Figure 5.7, we show the average OOB power leakage reduction of precoder B as a function of β, which represents the power overhead consumed by the free subcarriers relative to the data symbols, as well as the number of free subcarriers when the EVM is set to 8%. We choose 3 sets of free subcarriers where $N_{\mathrm{r}} = \{12, 18, 24\}$, with $N_{\mathrm{r}}/2$ subcarriers on each edge of the transmission band. Figure 5.7 clearly shows the improvement in the suppression performance as the number of free subcarriers increases. Another observation in Figure 5.7 is that, for a given number of free subcarriers, the average OOB power leakage reduction improves as β increases up to a point, after

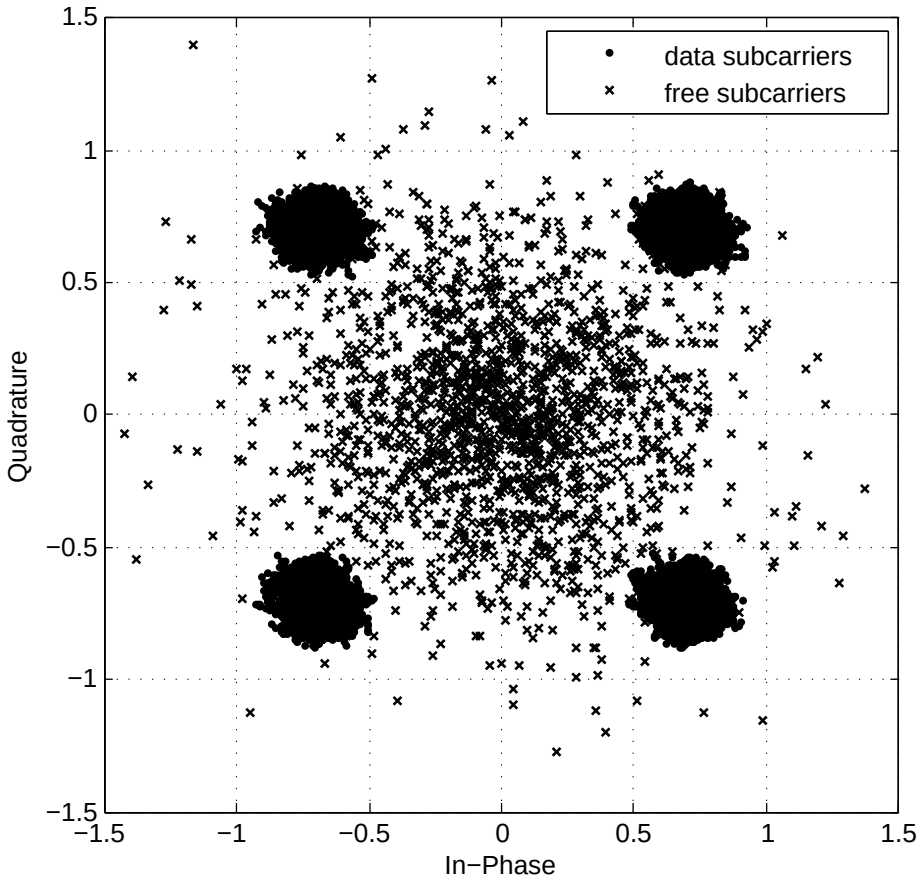

Figure 5.6 Constellation of 4-QAM symbols transmitted by precoder B, $\beta = 2\%, N_r = 18, \text{EVM} = 8\%$.

which, any increase in β does not translate in any improvement in the OOB emission reduction. This result can help in setting the power overhead for a given EVM and number of free subcarriers.

The actual PSD performance of precoder B is shown in Figure 5.8. The EVM is set to 8%, the number of free subcarriers is $N_r = 18$ with 9 subcarriers on each side of the transmission band and the free subcarriers have a 2% power overhead. For only a $18/300 = 6\%$ reduction in the transmission rate, precoder B can achieve deep suppression compared to precoder A for the same EVM of 8%.

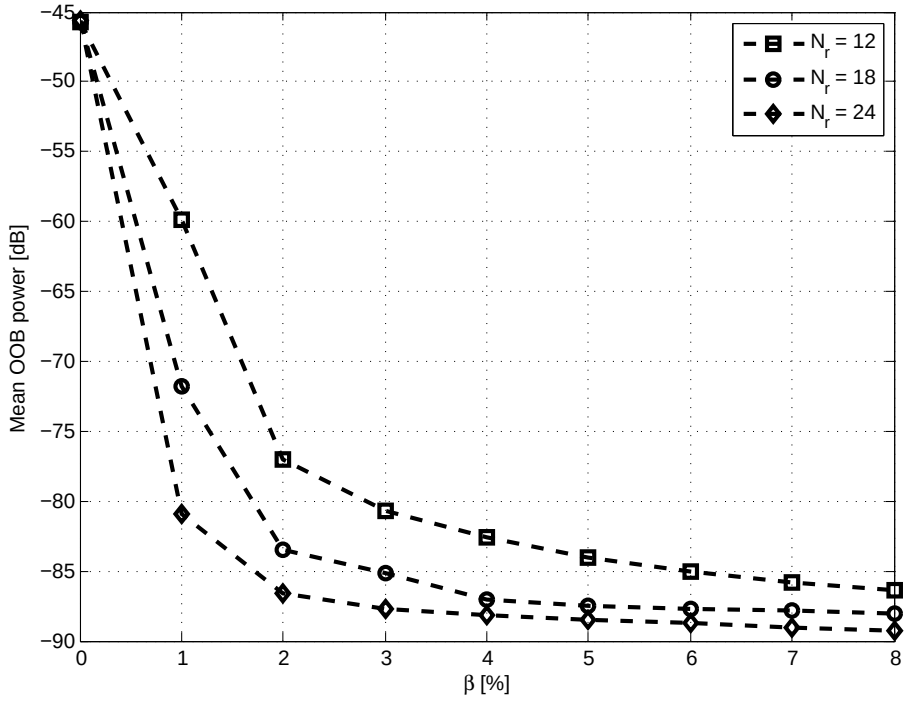

Figure 5.7 Mean OOB performance for precoder B, EVM = 8%.

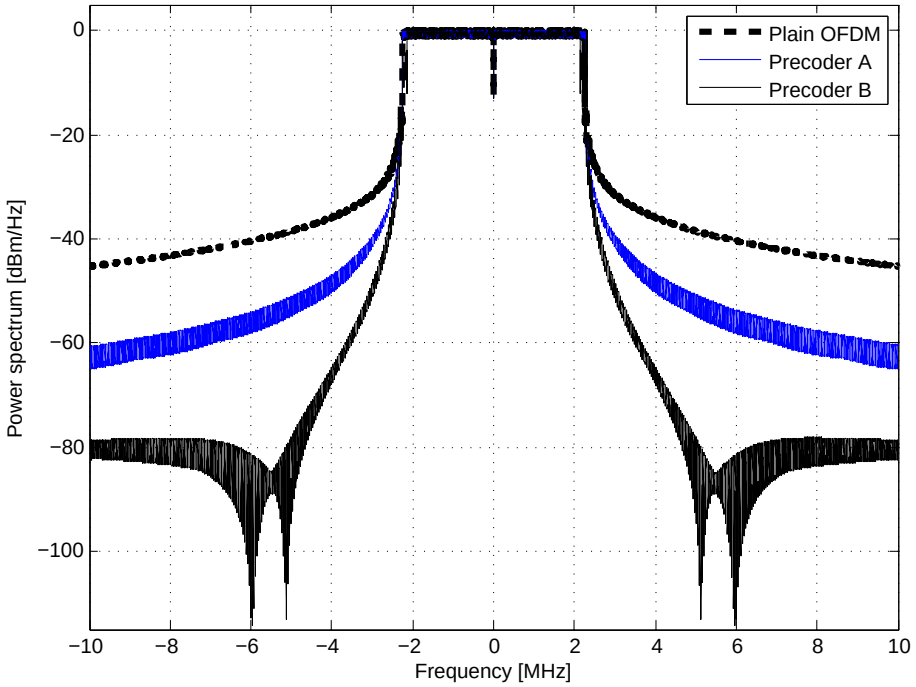

Figure 5.8 Performance of precoder A and precoder B, $\beta = 2\%, N_r = 18,$ EVM $= 8\%$ for 4-QAM.

5.5 Conclusion

In this chapter, we presented two precoders for improving the spectral emissions of OFDM. The proposed precoders can significantly reduce the OOB power leakage of the transmitted signal while guaranteeing acceptable error performance at the receiver without the need for transmitting any side information, thereby maintaining a transmission rate similar to that of plain OFDM. We also showed the improvement in the suppression performance of the proposed precoders compared to other state of the art precoders.

REFERENCES

[1] J. van de Beek, "Sculpting the multicarrier spectrum: a novel projection precoder," *IEEE Commun. Lett.*, vol. 13, no. 12, pp. 881–883, Dec. 2009.

[2] J. van de Beek and F. Berggren, "EVM-constrained OFDM precoding for reduction of out-of-band emission," in *Proc. IEEE Veh. Technol. Conf. (VTC)*, Sep. 2009, pp. 1–5.

[3] P. Kolodzy and I. Avoidance, "Spectrum policy task force," *Federal Commun. Comm., Washington, DC, Rep. ET Docket*, no. 02-135, 2002.

[4] J. Mitola, "Cognitive radio for flexible mobile multimedia communications," in *Mobile Multimedia Communications, 1999. (MoMuC '99) 1999 IEEE International Workshop on*, 1999, pp. 3–10.

[5] F. C. Commission *et al.*, "Unlicensed operation in the TV broadcast bands," *ET Docket*, no. 04-186, 2004.

[6] T. Yucek and H. Arslan, "A survey of spectrum sensing algorithms for cognitive radio applications," *Communications Surveys Tutorials, IEEE*, vol. 11, no. 1, pp. 116–130, First 2009.

[7] P. Siohan, C. Siclet, and N. Lacaille, "Analysis and design of ofdm/oqam systems based on filterbank theory," *Signal Processing, IEEE Transactions on*, vol. 50, no. 5, pp. 1170–1183, May 2002.

[8] N. Michailow, M. Matthe, I. Gaspar, A. Caldevilla, L. Mendes, A. Festag, and G. Fettweis, "Generalized frequency division multiplexing for 5th generation cellular networks," *Communications, IEEE Transactions on*, vol. 62, no. 9, pp. 3045–3061, Sept 2014.

[9] J. Bingham, "Multicarrier modulation for data transmission: an idea whose time has come," *Communications Magazine, IEEE*, vol. 28, no. 5, pp. 5–14, May 1990.

[10] D. Astely, E. Dahlman, A. Furuskar, Y. Jading, M. Lindstrom, and S. Parkvall, "LTE: the evolution of mobile broadband," *Communications Magazine, IEEE*, vol. 47, no. 4, pp. 44–51, April 2009.

[11] I. . W. Group *et al.*, "IEEE 802.11-2007: Wireless LAN medium access control (MAC) and physical layer (PHY) specifications," *IEEE 802.11 LAN Standards 2007*, 2007.

[12] F. Wang, A. Ghosh, C. Sankaran, P. Fleming, F. Hsieh, and S. Benes, "Mobile wimax systems: performance and evolution," *Communications Magazine, IEEE*, vol. 46, no. 10, pp. 41–49, October 2008.

[13] "IEEE Standard for Information Technology–Telecommunications and information exchange between systems Wireless Regional Area Networks (WRAN)–Specific requirements Part 22: Cognitive Wireless RAN Medium Access Control (MAC) and Physical Layer (PHY) Specifications: Policies and Procedures for Operation in the TV Bands," *IEEE Std 802.22-2011*, pp. 1–680, 1 2011.

[14] H. Chen and W. Gao, "MAC and PHY proposal for 802.11 af," 2010.

[15] A. B. Flores, R. E. Guerra, E. W. Knightly, P. Ecclesine, and S. Pandey, "IEEE 802.11 af: a standard for TV white space spectrum sharing." *IEEE Communications Magazine*, vol. 51, no. 10, pp. 92–100, 2013.

[16] E. Etsi, "300 744:" digital video broadcasting (DVB)," *Framing structure, channel coding and modulation for digital terrestrial television*, vol. 1, no. 2, 2004.

[17] E. ETSI, "300 401 v1. 4.1 (2006-06)," *Radio Broadcasting Systems.*

[18] L. Cimini, "Analysis and simulation of a digital mobile channel using orthogonal frequency division multiplexing," *IEEE Trans. Commun.*, vol. 33, no. 7, pp. 665–675, Jul. 1985.

[19] H. Mahmoud, T. Yucek, and H. Arslan, "OFDM for cognitive radio: merits and challenges," *IEEE Trans. Commun.*, vol. 16, no. 2, pp. 6–15, Apr. 2009.

[20] A. Şahin, I. Güvenç, and H. Arslan, "A survey on multicarrier communications: Prototype filters, lattice structures, and implementation aspects," *IEEE Commun. Surveys Tuts.*, vol. 16, no. 3, pp. 1312–1338, Third Quarter 2014.

[21] D. Qu, J. Ding, T. Jiang, and X. Sun, "Detection of non-contiguous OFDM symbols for cognitive radio systems without out-of-band spectrum synchronization," *IEEE Trans. Wireless Commun.*, vol. 10, no. 2, pp. 693–701, February. 2011.

[22] T. Jiang and Y. Wu, "An overview: Peak-to-average power ratio reduction techniques for OFDM signals," *IEEE Trans. Broadcasting.*, vol. 54, no. 2, pp. 257–268, June. 2008.

[23] E. Costa, M. Midrio, and S. Pupolin, "Impact of amplifier nonlinearities on OFDM transmission system performance," *IEEE Commun. Lett.*, vol. 3, no. 2, pp. 37–39, February. 1999.

[24] W. Chongburee, "Analysis of power spectral density of digitally-modulated combined pulse trains," in *Proceedings of the 2nd ECTI Annual Conference*, 2005.

[25] S. Slimane, "Reducing the peak-to-average power ratio of OFDM signals through precoding," *IEEE Trans. Veh. Technol.*, vol. 56, no. 2, pp. 686–695, Mar. 2007.

[26] X.-G. Xia, "Precoded and vector OFDM robust to channel spectral nulls and with reduced cyclic prefix length in single transmit antenna systems," *IEEE Trans. Commun.*, vol. 49, no. 8, pp. 1363–1374, Aug. 2001.

[27] M. Debbah, P. Loubaton, and M. de Courville, "Asymptotic performance of successive interference cancellation in the context of linear precoded OFDM systems," *IEEE Trans. Commun.*, vol. 52, no. 9, pp. 1444–1448, Sep. 2004.

[28] J. Zhang, X. Huang, A. Cantoni, and Y. Guo, "Sidelobe suppression with orthogonal projection for multicarrier systems," *IEEE Trans. Commun.*, vol. 60, no. 2, pp. 589–599, Aug. 2012.

[29] J. van de Beek, "Orthogonal multiplexing in a subspace of frequency well-localized signals," *IEEE Commun. Lett.*, vol. 14, no. 10, pp. 882–884, Oct. 2010.

[30] M. Ma, X. Huang, B. Jiao, and Y. Guo, "Optimal orthogonal precoding for power leakage suppression in DFT-based systems," *IEEE Trans. Commun.*, vol. 59, no. 3, pp. 844–853, Mar. 2011.

[31] J. Van De Beek and F. Berggren, "N-continuous OFDM," *IEEE Commun. Lett.*, vol. 13, no. 1, pp. 1–3, Jan. 2009.

[32] Y. Zheng, J. Zhong, M. Zhao, and Y. Cai, "A precoding scheme for N-continuous OFDM," *IEEE Commun. Lett.*, vol. 16, no. 12, pp. 1937–1940, Dec. 2012.

[33] C.-D. Chung, "Correlatively coded OFDM," *IEEE Trans. Wireless Commun.*, vol. 5, no. 8, pp. 2044–2049, Aug. 2006.

[34] ——, "Spectrally precoded OFDM," *IEEE Trans. Commun.*, vol. 54, no. 12, pp. 2173–2185, Dec. 2006.

[35] ——, "Spectral precoding for rectangularly pulsed OFDM," *IEEE Trans. Commun.*, vol. 56, no. 9, pp. 1498–1510, Sep. 2008.

[36] ——, "Spectral precoding for constant-envelope OFDM," *IEEE Trans. Commun.*, vol. 58, no. 2, pp. 555–567, Feb. 2010.

[37] H.-M. Chen, W.-C. Chen, and C.-D. Chung, "Spectrally precoded OFDM and OFDMA with cyclic prefix and unconstrained guard ratios," *IEEE Trans. Wireless Commun.*, vol. 10, no. 5, pp. 1416–1427, May. 2011.

[38] R. Xu and M. Chen, "A precoding scheme for DFT-based OFDM to suppress sidelobes," *IEEE Commun. Lett.*, vol. 13, no. 10, pp. 776–778, Oct. 2009.

[39] G. Strang, *Linear Algebra and its Applications.* Academic Press, 1976.

[40] I. Cosovic, S. Brandes, and M. Schnell, "Subcarrier weighting: a method for sidelobe suppression in OFDM systems," *IEEE Commun. Lett.*, vol. 10, no. 6, pp. 444–446, Jun. 2006.

[41] ——, "A technique for sidelobe suppression in OFDM systems," in *Proc. IEEE Global Telecommun. Conf. (GLOBECOM)*, vol. 1, 2005, pp. 1–5.

[42] X. Fu, J. Wang, and S.-Q. Li, "Sidelobe suppression for OFDM based cognitive radio systems," in *Proc. IEEE International Conference on Communications and Networking in China (CHINACOM)*, 2009, pp. 1–5.

[43] E. Lawrey and C. Kikkert, "Peak to average power ratio reduction of OFDM signals using peak reduction carriers," in *Proc. IEEE International Symposium on Signal Processing and Its Applications (ISSPA)*, vol. 2, Aug. 1999, pp. 737–740.

[44] M. Senst, M. Jordan, M. Dorpinghaus, M. Farber, G. Ascheid, and H. Meyr, "Joint reduction of peak-to-average power ratio and out-of-band power in OFDM systems," in *Proc. IEEE Global Telecommun. Conf. (GLOBECOM)*, 2007, pp. 3812–3816.

[45] S. Brandes, I. Cosovic, and M. Schnell, "Reduction of out-of-band radiation in OFDM systems by insertion of cancellation carriers," *IEEE Commun. Lett.*, vol. 10, no. 6, pp. 420–422, Jun. 2006.

[46] ——, "Sidelobe suppression in OFDM systems by insertion of cancellation carriers," in *Proc. IEEE Vehic. Technol. Conf. (VTC)*, vol. 1, 2005, pp. 152–156.

[47] J. A. C. Bingham, "RFI suppression in multicarrier transmission systems," in *Proc. IEEE Global Telecommun. Conf. (GLOBECOM)*, vol. 2, 1996, pp. 1026–1030.

[48] H. Mahmoud and H. Arslan, "Spectrum shaping of OFDM-based cognitive radio signals," in *Proc. IEEE Radio and Wireless Symposium (RWS)*, 2008, pp. 113–116.

[49] J. van de Beek and F. Berggren, "Out-of-band power suppression in OFDM," *IEEE Commun. Lett.*, vol. 12, no. 9, pp. 609–611, Sep. 2008.

[50] E. Alian and P. Mitran, "Improved active interference cancellation for sidelobe suppression in cognitive OFDM systems," in *Proc. IEEE Global Communications Conference (GLOBECOM)*, Dec. 2012, pp. 1460–1465.

[51] T. Matsuura, Y. Iida, C. Han, and T. Hashimoto, "Improved algorithms for cancellation carrier optimization to suppress the OFDM OOB spectrum," *IEEE Commun. Lett.*, vol. 13, no. 2, pp. 112–114, Feb. 2009.

[52] H. Yamaguchi, "Active interference cancellation technique for MB-OFDM cognitive radio," in *Proc. IEEE European Microwave Conference*, vol. 2, 2004, pp. 1105–1108.

[53] D. Qu, Z. Wang, and T. Jiang, "Extended active interference cancellation for sidelobe suppression in cognitive radio OFDM systems with cyclic prefix," *IEEE Trans. Vehicular. Technol.*, vol. 59, no. 4, pp. 1689–1695, May. 2010.

[54] T. Weiss, J. Hillenbrand, A. Krohn, and F. Jondral, "Mutual interference in OFDM-based spectrum pooling systems," in *Proc. IEEE Vehic. Technol. Conf. (VTC)*, vol. 4, May 2004, pp. 1873–1877.

[55] H. Mahmoud and H. Arslan, "Sidelobe suppression in OFDM-based spectrum sharing systems using adaptive symbol transition," *IEEE Commun. Lett.*, vol. 12, no. 2, pp. 133–135, Feb. 2008.

[56] A. Sahin and H. Arslan, "Edge windowing for OFDM based systems," *IEEE Commun. Lett.*, vol. 15, no. 11, pp. 1208–1211, Nov. 2011.

[57] ——, "The impact of scheduling on edge windowing," in *Proc. IEEE Global Telecommun. Conf. (GLOBECOM)*, 2011, pp. 1–5.

[58] B. Farhang-Boroujeny, "OFDM versus filter bank multicarrier," *IEEE Sig. Proc. Mag.*, vol. 28, no. 3, pp. 92–112, May 2011.

[59] R. Datta, M. Gautier, V. Berg, Y. Futatsugi, M. Ariyoshi, M. Schuhler, Z. Kollar, P. Horvath, D. Noguet, and G. Fettweis, "Flexible multicarrier phy design for cognitive radio in white space," in *Proc. IEEE Int. Conf. Cognitive Radio Oriented Wireless Networks and Commun. (CROWNCOM)*, 2011, pp. 141–145.

[60] A. Tom, A. Sahin, and H. Arslan, "Mask compliant precoder for OFDM spectrum shaping," *IEEE Commun. Lett.*, vol. 17, no. 3, pp. 447–450, Mar. 2013.

[61] N. Gould and P. L. Toint, "Preprocessing for quadratic programming," *Math. Program.*, vol. 100, no. 1, pp. 95–132, May 2004.

[62] A. Ghassemi, L. Lampe, A. Attar, and T. Gulliver, "Joint sidelobe and peak power reduction in ofdm-based cognitive radio," in *IEEE Veh. Technol. Conf. (VTC)*, Sept. 2010, pp. 1–5.

[63] E. Guvenkaya, A. Tom, and H. Arslan, "Joint sidelobe suppression and papr reduction in OFDM using partial transmit sequences," in *Military Communications Conference, MILCOM 2013 - 2013 IEEE*, Nov. 2013, pp. 95–100.

[64] C. Ni, T. Jiang, and W. Peng, "Joint papr reduction and sidelobe suppression using signal cancellation in NC-OFDM based cognitive radio systems," *IEEE Trans. Vehicular Technol*, vol. PP, no. 99, pp. 1–1, 2014.

[65] M. Maso, M. Debbah, and L. Vangelista, "A distributed approach to interference alignment in OFDM-based two-tiered networks," *IEEE Trans. Vehicular Technol.*, vol. 62, no. 5, pp. 1935–1949, Jun. 2013.

[66] H. Qin, Y. Sun, T.-H. Chang, X. Chen, C.-Y. Chi, M. Zhao, and J. Wang, "Power allocation and time-domain artificial noise design for wiretap OFDM with discrete inputs," *IEEE Trans. Wireless Commun.*, vol. 12, no. 6, pp. 2717–2729, Jun. 2013.

[67] M. Maso, S. Lakshminarayana, T. Quek, and H. Poor, "A composite approach to self-sustainable transmissions: Rethinking OFDM," *IEEE Trans. Commun.*, vol. PP, no. 99, pp. 1–1, 2014.

[68] V. Cadambe and S. Jafar, "Interference alignment and degrees of freedom of the k-user interference channel," *IEEE Trans. Information Theory.*, vol. 54, no. 8, pp. 3425–3441, Aug. 2008.

[69] S. Boyd and L. Vandenberghe, *Convex Optimization*. New York, NY, USA: Cambridge University Press, 2004.

[70] J. Löfberg, "YALMIP : a toolbox for modeling and optimization in MATLAB," in *Proc. IEEE International Symposium on Computer Aided Control Systems Design (CACSD)*, Sep. 2004, pp. 284–289.

[71] MOSEK. [Online]. Available: http://www.mosek.com

[72] S. Ye, R. Blum, and L. Cimini, "Adaptive OFDM systems with imperfect channel state information," *IEEE Trans. Wireless Commun.*, vol. 5, no. 11, pp. 3255–3265, November 2006.

[73] R. Hassun, M. Flaherty, R. Matreci, and M. Taylor, "Effective evaluation of link quality using error vector magnitude techniques," in *Wireless Communications Conference, 1997., Proceedings*, Aug 1997, pp. 89–94.

[74] R. Shafik, S. Rahman, R. Islam, and N. Ashraf, "On the error vector magnitude as a performance metric and comparative analysis," in *Emerging Technologies, 2006. ICET '06. International Conference on*, Nov 2006, pp. 27–31.

[75] "Supplement to IEEE standard for information technology - telecommunications and information exchange between systems - local and metropolitan area networks - specific requirements. part 11: Wireless LAN medium access control (MAC) and physical layer (PHY) specifications: High-speed physical layer in the 5 ghz band," *IEEE Std 802.11a-1999*, pp. i–, 1999.

[76] K. B. Petersen and M. S. Pedersen, "The matrix cookbook."

APPENDICES

Appendix A : Acronyms

Acronym	Description
3GPP	3rd Generation Partnership Project
ACLR	adjacent channel leakage ratio
AIC	active interference cancellation
AWGN	additive white Gaussian noise
BER	bit error rate
CCDF	complimentary cumulative distribution function
CC	cancellation carriers
CP	cyclic prefix
CR	cognitive radio
CSI	channel state information
DFT	discrete Fourier transformation
EVM	error vector magnitude
FBMC	filter bank multicarrier
FCC	Federal Communication Commission
FFT	fast Fourier transformation
GFDM	generalized frequency division multiplexing
IA	interference alignment
ICI	inter-carrier interference
IDFT	inverse discrete Fourier transformation
IFFT	inverse fast Fourier transformation
ISI	inter-symbol interference
LSQI	least squares with a quadratic inequality
MSE	mean square error
OFDM	Orthogonal frequency division multiplexing
OOB	out-of-band

Acronym	Description
PA	power amplifier
PAPR	peak-to-average power ratio
PDP	power delay profile
PHY	physical layer
PSD	power spectral density interference
P/S	parallel-to-serial
PU	primary user
RF	radio frequency
RRC	root-raised cosine
SA	suppressing alignment
SEM	spectral emission mask
SNR	signal-to-noise ratio
S/P	serial-to-parallel
SU	secondary user
SW	subcarrier weighting

Appendix B : Copyrights Notice

The permission below is for the material in Chapter (3).

Copyright Clearance Center RightsLink® Home Create Account Help Live Chat

IEEE Requesting permission to reuse content from an IEEE publication

Title: Mask Compliant Precoder for OFDM Spectrum Shaping
Author: Tom, A.; Sahin, A.; Arslan, H.
Publication: IEEE Communications Letters
Publisher: IEEE
Date: March 2013

LOGIN
If you're a copyright.com user, you can login to RightsLink using your copyright.com credentials. Already **a RightsLink user** or want to learn more?

Thesis / Dissertation Reuse

The IEEE does not require individuals working on a thesis to obtain a formal reuse license, however, you may print out this statement to be used as a permission grant:

Requirements to be followed when using any portion (e.g., figure, graph, table, or textual material) of an IEEE copyrighted paper in a thesis:

1) In the case of textual material (e.g., using short quotes or referring to the work within these papers) users must give full credit to the original source (author, paper, publication) followed by the IEEE copyright line © 2011 IEEE.
2) In the case of illustrations or tabular material, we require that the copyright line © [Year of original publication] IEEE appear prominently with each reprinted figure and/or table.
3) If a substantial portion of the original paper is to be used, and if you are not the senior author, also obtain the senior author's approval.

Requirements to be followed when using an entire IEEE copyrighted paper in a thesis:

1) The following IEEE copyright/ credit notice should be placed prominently in the references: © [year of original publication] IEEE. Reprinted, with permission, from [author names, paper title, IEEE publication title, and month/year of publication]
2) Only the accepted version of an IEEE copyrighted paper can be used when posting the paper or your thesis on-line.
3) In placing the thesis on the author's university website, please display the following message in a prominent place on the website: In reference to IEEE copyrighted material which is used with permission in this thesis, the IEEE does not endorse any of [university/educational entity's name goes here]'s products or services. Internal or personal use of this material is permitted. If interested in reprinting/republishing IEEE copyrighted material for advertising or promotional purposes or for creating new collective works for resale or redistribution, please go to http://www.ieee.org/publications_standards/publications/rights/rights_link.html to learn how to obtain a License from RightsLink.

If applicable, University Microfilms and/or ProQuest Library, or the Archives of Canada may supply single copies of the dissertation.

BACK CLOSE WINDOW

ABOUT THE AUTHOR

Anas Tom received his B.Sc. degree in electrical engineering from the University of Khartoum, Khartoum, Sudan and his M.Sc. degree in electrical engineering from Southern Illinois University, Carbondale, IL USA. He was previously with Huawei Technologies as a wireless engineer. He is currently working towards his Ph.D degree in electrical engineering at the University of South Florida, Tampa, FL USA. His research interests include interference reduction for OFDM-based systems, spectrum shaping for cognitive radio and interference alignment.